Stageverslag

Evaluation of the diurnal cycle of trace gases over Beijing as modelled by CHIMERE

A. Lampe

De Bilt, 2009

KNMI stageverslag

De Bilt, 2009

PO Box 201
3730 AE De Bilt
Wilhelminalaan 10
De Bilt
The Netherlands
http://www.knmi.nl
Telephone +31(0)30-220 69 11
Telefax +31(0)30-221 04 07

Auteur: Lampe, A.

Master Thesis Report

Evaluation of the Diurnal Cycle of Trace Gases over Beijing as Modelled by Chimere

Arjan Lampe

July 7, 2009

Supervisors:
Prof. dr. ir. H.W.M. Hoeijmakers
Prof. dr. H.M. Kelder
dr. R.J. van der A

Master Thesis Report:
'Evaluation of the Diurnal Cycle of Trace Gases over Beijing as Modelled by Chimere'
Author: Arjan Lampe

Supervisors:
Prof. dr. ir. H.W.M. Hoeijmakers
Prof. dr. H.M. Kelder
dr. R.J. van der A

University of Twente
Mechanical Engineering
Faculty of *'Engineering Technology'*
Drienerlolaan 5
PO box 217
7500 AE Enschede

Enschede, July 7, 2009
Master Thesis Report
Report: 61 pages
Printing: 7

Abstract

In the framework of the international EU and ESA project "Air quality Monitoring and Forecasting In China" (AMFIC) an air quality forecast system of Eastern China is in development.

Chimere is the chemical transport model used for this purpose. It has meteorological forecasts and emissions as inputs and calculates through advection and chemical reactions of 44 species their temporal and spatial concentrations in a computational domain.

The model output of Chimere is compared to in situ measurements of pollutants in Beijing, showing that the predicted nocturnal concentrations of pollutants are systematically too high. The objective of the present research is to find possible causes of this discrepancy. To achieve this goal several sensitivity studies of parameters in the model have been conducted. These studies show that the discrepancy is due to the incorrect representation of the atmospheric boundary layer height. This is due to the absence of the so-called urban heat island effect in Chimere. The urban heat island is the phenomenon of the air inside an urban region being warmer than its rural surroundings. This effect is strongest at night and increases vertical mixing resulting in a higher nocturnal atmospheric boundary layer. It is shown that incorporating this effect in the Chimere model leads to a better agreement of the calculated surface pollutant concentrations with observations.

Contents

1 Introduction

The economy of China has grown enormously in the last two decades. This rapid growth has as consequence a large growth in air pollution. Most economical activities are concentrated in megacities like Beijing (around 17 million inhabitants), Shanghai (around 19 million inhabitants, largest city of China) and Hong Kong (around 7 million inhabitants). This causes emissions to be concentrated in small and dense areas creating heavy pollution causing health problems. This is a major concern for society and therefore also for local and international authorities.

One of the challenges is of how to reduce the air pollution in such cities and their surroundings. In that light it is quite stimulating that the effects of a change in policy or measures like those imposed during the Olympic Games of 2008 are clearly visible and effective. To monitor these changes the international EU and ESA project Air quality Monitoring and Forecasting In China (AMFIC, see `www.amfic.eu`) has been initiated. It has as objective to setup and test an air quality forecast system for Eastern China.

For the forecasting the chemical transport model Chimere (see `www.lmd.poly technique.fr/chimere`) is used. Chimere is a model developed at the 'Laboratoire de Météorologie Dynamique' (laboratory of dynamical meteorology) of the École Polythechnique, the Institut National de l'Environnement industriel et des risques and LISA University, all in and around Paris. It uses as input meteorological data e.g. wind fields, temperature, humidity, etc., and emission data, e.g. emission of many pollutants per hour of the day due to traffic or industry but also due to biomass. By calculating the transport, the chemical reactions and the sinks of 44 pollutants Chimere simulates the concentrations of, amongst many others, particulate matter (PM10, concentrations are measured in number of particles per volume, the 10 refers to the maximum size in μm), nitrogen-(di)oxide (NOx), carbon-monoxide (CO) and ozone (O_3) per grid cell per hour of the day. The high resolution domain of Chimere stretches from 18° to 52° North, and from 102° to 132° East. This domain has been chosen because the population density and thus the pollution is by far the greatest in this part of China.

The observed surface concentrations of most pollutants have a diurnal cycle, e.g. PM10 and NO can show local maxima in concentration during rush hours because a large source is traffic. Because O_3 is created by a chemical reaction involving sunlight, its surface concentration is highest during the day and smallest during the night. During the night it reacts with NO to form NO_2 and almost disappears.

Chimere model results also show a diurnal cycle, albeit not entirely the same as the diurnal cycle of the measured concentrations. Remarkable is a sharp increase around sunset and a sharp decrease around sunrise. The measurements show a more constant trend. Also the nocturnal concentrations are much higher compared to measurements.

The goal of this thesis is to find causes of these overestimated modelled nocturnal concentrations and to see if they can be corrected. This will be done by running the model under different setups and comparing the result with in situ measurements.

1.1 Problem Statement

Ground measurements of pollutants from China are rare, this is even more true for measurements of the diurnal cycle. One of the few publications of a measured diurnal cycle is [Wang et al. (2008)]. This study will be used to compare the results of Chimere with.

In the period from the 7th of August until the 30th of September in 2007 in-situ measurements have been carried out of the concentrations of gases relevant for air quality which is reported in [Wang et al. (2008)]. The sampling instruments were installed on the roof of a $15\,m$ building of the Chinese Research Academy of Environmental Sciences in Beijing. The building is located near a residential area in the Northern part of Beijing (40°02' N, 116°24' E). There are no industrial air pollution sources nearby. Figure 1.1A shows the plot presented in [Wang et al. (2008)] showing the diurnal cycle averaged over August and September 2007.

For the same period a simulation has been carried out with Chimere. This simulation uses the 12 hour ECMWF forecasts which represent the weather as it was in this period as good as possible. The model output of the lowest vertical layer is interpolated to the Olympic Park in Beijing using bilinear interpolation. The data of [Wang et al. (2008)] is representable for this area. The results are plotted in figure 1.1B.

Comparison of measured concentrations (fig. 1.1A) with modelled concentrations (fig. 1.1B) leads to the following conclusions:

- The concentrations of NO and NO2 are comparable during the day.
- Both the modelled PM10 and CO concentrations are lower than measured data during the day.
- Modelled SO2 emissions are higher compared with measured data, both during the day and during the night.
- The averaged concentrations of ozone are quite well represented by the model.
- The model results show a sharp increase at sunset and a sharp decrease at sunrise resulting in too high nocturnal pollutant concentrations.

The emissions of PM10 are much lower during the night. This is because its main source is traffic which is less intense during the night, see figure 1.2. The measurements however do not show a decrease in concentration in this period, they even show a slight increase. In contrast all the modelled concentrations except for ozone show a much sharper rise at the start of the night and a sharp decrease at the end of the night. The measured concentrations do not show this behavior qualitatively. In this study we will explain this discrepancy.

One important observation can be made here already. The nightly increase of concentrations as produced by the model occurs for every species, also PM10. PM10 is chemically not very active and long-lived. This means that the problem is dynamically in nature, not chemically. This is the reason this study's focus is on PM10 concentrations and chemistry is not taken into account.

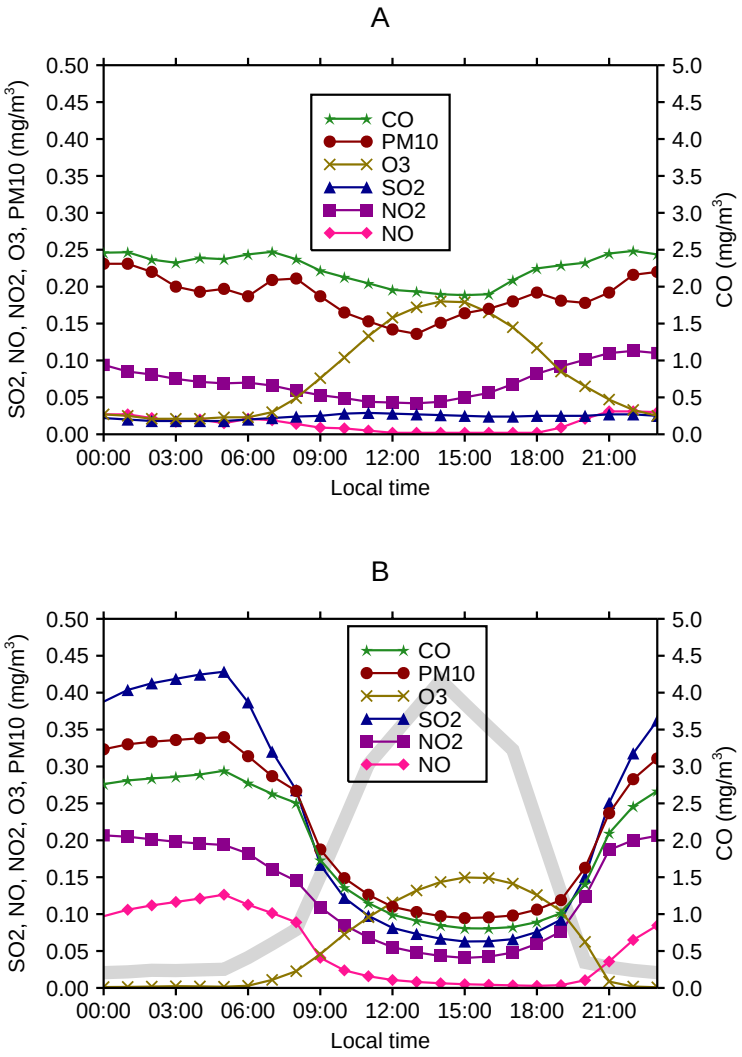

Figure 1.1: Measured concentrations from the building of the Chinese Research Academy of Environmental Sciences in Beijing, from [Wang et al.(2008)] (above). And modelled concentrations interpolated to the Olympic Park in Beijing (below). The grey thick line on the background is the boundary layer height as used in the model. Its maximum is around 1800 m. Both plots show averaged values over August and September 2007

1.2 Scope

To limit the research conducted in this report a scope is defined which is presented here. Not withstanding chemistry calculations are a main feature of Chimere, its effects will be avoided as much as possible. Only dynamical features will be explored. This is no limitation because it will be shown the discrepancy between measured and modelled night concentrations can be explained by dynamical effects.

The atmospheric boundary layer height is an important parameter for the

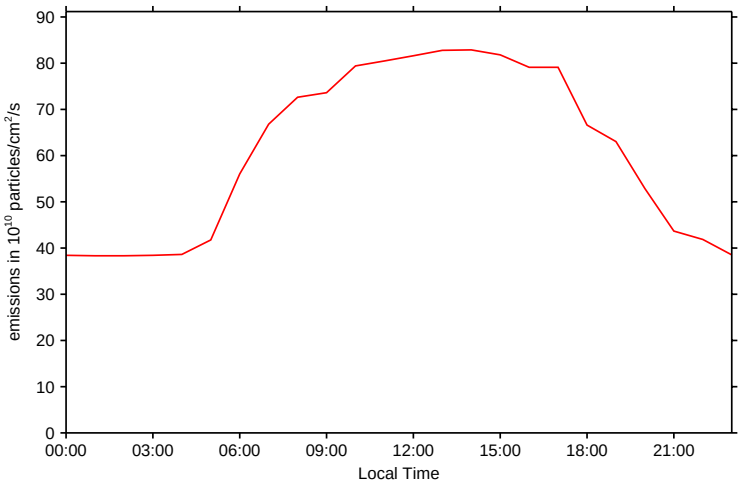

Figure 1.2: PM10 emissions interpolated to Beijing as implemented in the model for a midweek day.

calculation of pollutant concentrations. Much complications in the calculation of the boundary layer height arise when clouds are present or start to form. However, it is shown in this report that the forming of an urban heat island (a temperature difference between the city and its surroundings) can explain the discrepancy. This effect is strongest when no clouds are present. This is why no clouds or forming of clouds are taken into account in this study.

1.3 Report Outline

To understand how Chimere calculates the concentrations of the different species, chapter 2 is devoted to explaining the details of the model. The boundary layer and vertical diffusion coefficient are very important parameters of the problem. The theory behind these parameters and how they are implemented in the model is explained in chapter 3. After this the results of different simulations are presented in chapter 4. It will be concluded that the effect of cities on the boundary layer height and the vertical diffusion coefficient is missing in the model. How these parameters are affected and how they might be modelled is presented in chapter 5.

2 Chimere

Chimere is a chemical transport model used to numerically simulate the concentrations of different trace gases and aerosols within its computational domain. Here details about how the model calculates species concentrations are given.

The core of a chemical transport model like Chimere is shown in figure 2.1. It calculates the fluxes due to transport, the emissions, the depositions and the production and loss due to chemistry. Transport is mainly due to advection but in the lowest part of the atmosphere, known as the atmospheric boundary layer, vertical dispersion due to turbulence is also taken into account. Depositions can be of two forms: dry and wet deposition. Dry depositions occurs when plants or water absorb gases, wet deposition is when pollutants are washed out due to precipitation. Chimere has a very sophisticated chemical module which takes the chemical interaction between 44 species through about 120 reactions into account.

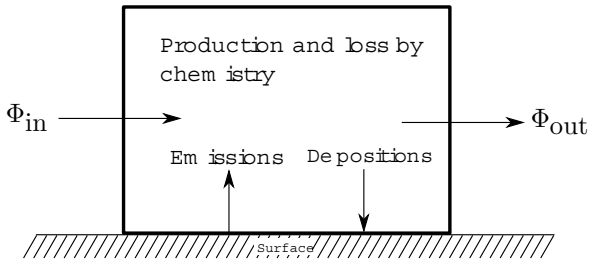

Figure 2.1: The production and loss terms of a surface level grid cell. Φ is the flux of a certain species.

2.1 Model Input

Chimere needs information to be able to carry out a numerical simulation. Which information Chimere needs and its source is listed below.

Meteorology Chimere uses meteorological data—wind fields, humidity, temperature, precipitation, cloud fractions etc.—as input. In our case the 12 hour meteo forecasts of the 'European Center for Medium-range Weather Forecasts' (ECMWF) are used as a representation of the real weather during the summer of 2007 which resembles reality as good as possible. ECMWF provides data every three hours and since Chimere needs hourly data, time interpolation of the data is necessary. For this linear interpolation is used. The horizontal grid is exactly the same as used by Chimere.

Chimere can either calculate the boundary layer height itself from the meteorological data or it can take this from the ECMWF data. However, the developers of Chimere recommend to use data from meteorological models like that of ECMWF. Chimere calculates the vertical diffusion coefficient itself, see section 3.6.

Boundary conditions At the boundaries of the domain concentrations of the pollutants are prescribed. There are two sources for this data. The first is

a previous run of Chimere itself. In that case Chimere must have been run on a larger domain, the current run is then nested in this domain. The second source is monthly averaged data provided by the LMDZ-INCA2[1] model and the GOCART[2] model. The first model provides data for trace gasses, the latter for aerosols. This data is provided in the first case by the 'Institut Pierre-Simon Laplace' at Versailles. In the case of aerosols the data has been provided by Mian Chin from NASA.

The boundaries of the AMFIC domain are in areas where concentrations are low. This makes the sensitivity for boundary conditions low.

Initial conditions The initial conditions are either to be provided by a previous run of Chimere on a larger domain or by interpolation from the boundary conditions. Thus a certain startup time is needed to become insensitive for the initial conditions. In this study five days are used.

Land use Land use data is provided by the 'Global Land Cover Facility' (GLCF) which is a section of the University of Maryland. The data has a resolution of 1x1 km. This is converted to a file which contains per surface grid cell the percentage of a certain type of land cover, e.g. urban, grassland, forest, ocean, etc.

Emissions For the emissions the Asian database from the NASA 'INTEX-B' mission for 2006 is used. This dataset needs to be adapted before it can be used by Chimere. The database only gives estimated yearly emissions of a certain pollutant in a certain category (i.e. 'transportation', 'power', 'industry' and 'residence'). To convert this to hourly data, a daily profile per category is assumed for a midweek day, a Saturday and a Sunday. A seasonal trend is not yet implemented. Figure 2.2 shows the emissions of PM10 averaged over a midweek day in a region around Beijing.

As output Chimere gives the simulated concentrations of the 44 species it tracks for every grid cell and for each hour of the simulation time. Chimere also produces output files of emissions per species per surface tile in its domain and per hour. Furthermore the model also produces hourly values of the used meteorological parameters.

2.2 Model setup

For the simulations as used currently for the AMFIC forecasts, Chimere uses a regular grid of 121 points in longitude (x) direction and 129 points in latitude (y) direction. Every grid cell is 0.25° degrees in both x and y direction. The grid is placed in a domain that stretches from 18° to 52 ° North, and from 102° to 132° East. See figure 2.3.

[1] INCA is a chemistry and aerosol model coupled to the Laboratoire de Météorologie Dynamique (LMD) General Circulation Model, LMDz. INCA is developed at the Laboratoire des Sciences du Cimat et de l'Environnement (LSCE), see `http://www-lsceinca.cea.fr/index_UK.htm`.

[2] The Goddard Chemistry Aerosol Radiation and Transport (GOCART) model simulates major tropospheric aerosol components on a global scale. See `http://acdb-ext.gsfc.nasa.gov/People/Chin/gocartinfo.html`.

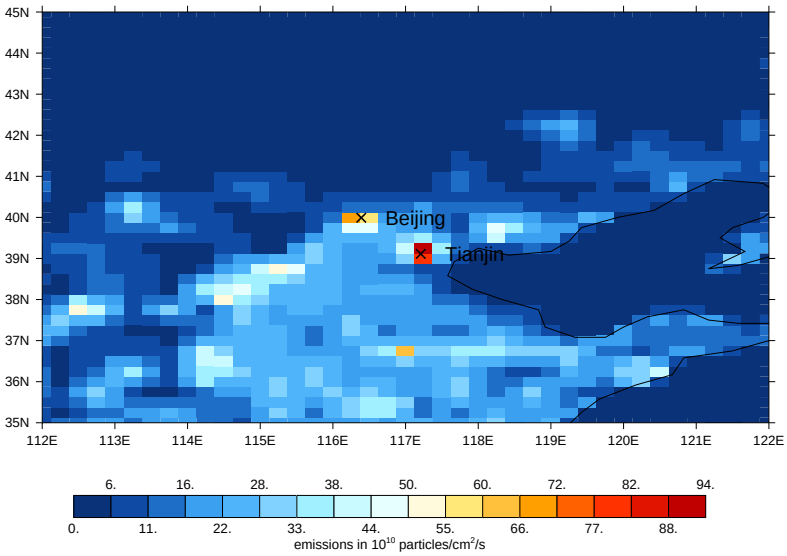

Figure 2.2: Emissions of PM10 in a region around Beijing averaged over a midweek day. Most other pollutants show a similar spread of emissions.

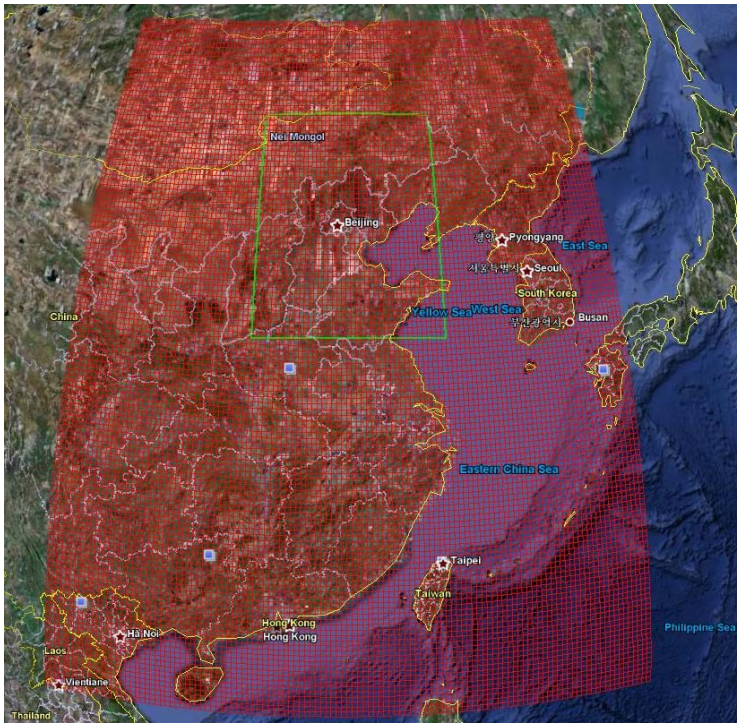

Figure 2.3: In red the grid as used by Chimere for the AMFIC forecasts superimposed on the map from Google Earth. In green is the grid used for several nested simulations. Courtesy B. Mijling

The grid has eight vertical layers. These layers increase in thickness with height, thus near the surface the grid has the highest resolution. Chimere uses for the vertical coordinate pressure instead of height above the surface, for the relation between pressure and height the hydrostatic equation (eq. 3.8) can be used. The pressure of layer i is defined using hybrid sigma-p coefficients

$$p_i = \sigma_{a,i} + \sigma_{b,i} p_0$$

where p_i is the pressure of the center of layer i, $\sigma_{a,i}$ and $\sigma_{b,i}$ are predefined constants for level i and p_0 is the surface pressure provided by the ECMWF forecasts. For the surface layer $\sigma_{a,i} = 0$ and $\sigma_{b,i} = 0.995$. This means that the lowest grid layer follows the topography of the land and its center is close to the surface. For the highest level $\sigma_{a,i} = 500\,hPa$ and $\sigma_{b,i} = 0$. This ensures that at the top of the domain the horizontal grid is on a constant pressure surface. Thus $500\,hPa$ is the center of the highest layer of the grid. When the surface pressure is $1000\,hPa$ the next table provides the height of the top of each layer.

layer	**pressure** [**hPa**]	**height** [**m**]
1	995	42
2	986	117
3	972	244
4	947	466
5	905	857
6	833	1569
7	710	2939
8	500	5942

2.3 Numerical Aspects

Chimere calculates advection and, inside the atmospheric boundary layer, turbulent dispersion of pollutants. Chimere also takes chemical reactions into account according to the MELCHIOR mechanism (see [Chimere Documentation] for details). This is a very sophisticated model which takes 44 species and about 120 reactions into account. However, as noted in section 1.1, the discrepancy between measurements and model results are dynamical of origin. This is why no further attention will be given to the chemical module.

Chimere has two methods to calculate horizontal advection. Which one it uses is dependent on the lifetime of the pollutant. In the case of a short-lived pollutant, e.g. ozone, an UPWIND discretization is used. In the other case, e.g. PM10, the Piecewise Parabolic Method is employed [Colella and Woodward, 1984].

Vertical advection is derived by calculating the budget of the horizontal mass fluxes and balancing this by a vertical mass flux, starting at the lowest grid level.

Some species are absorbed by vegetation or water. This is modelled by dry deposition with the help of three resistances. The first represents a resistance for the pollutant to be transported from far away to very close to the surface where it is being absorbed (R_t, only dependent on vertical (turbulent) flux). The second resistance accounts for the laminar resistance until upon the surface ($R_{l,i}$, this depends on molecular diffusion and thus on the species). The last resistance depends on the rate at which the surface can absorb the species $R_{a,i}$.

Thus the flux for dry deposition is parameterized as $F_i = v_i c_i$ with c_i the concentration of species i and

$$v_i = \frac{1}{R_t + R_{l,i} + R_{a,i}}$$

Wet deposition is the process in which the pollutant is washed out. This depends on the amount of precipitation.

Horizontal turbulent diffusion is not taken into account (it is assumed to be negligible compared to horizontal advection). Vertical turbulent diffusion is only important within the atmospheric boundary layer (ABL). This is parameterized by a model using K-diffusion theory, deduced by [Troen and Mahrt, 1986]. See chapter 3 for details.

Time integration is performed by an adapted variant of the TWOSTEP method, see figure 2.4. First all production (P) and loss (L) terms are calculated. Processes contributing to the production term could be chemical production, emissions but also advection. Processes contributing to the loss term could be wet and dry deposition and advection as well. When P and L are calculated the new concentrations are calculated using the TWOSTEP method.

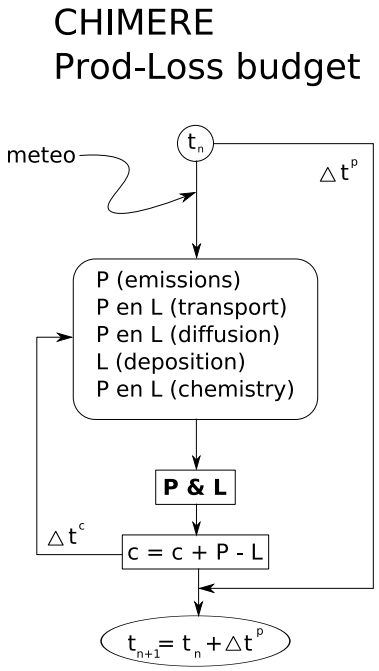

Figure 2.4: The numerical scheme as used by Chimere. At a physical time step t^n meteorological quantities are being updated. Then all the production and loss terms are calculated and concentrations c are calculated. This is repeated n times during the chemical time step for which $n\Delta t^c = \Delta t^p$. Then the physical time step is updated, $t_{n+1} = t_n + \Delta t^p$, and new meteorological quantities are loaded again. Adapted from [Chimere documentation].

Chimere uses two time steps. A physical time step (Δt^p, 10 minutes in our simulations) during which all physical quantities are being updated and a possibly smaller chemical time step (Δt^c, also 10 minutes in our simulations).

The latter is always a whole number of sub-steps of the physical time step. During the chemical time step all physical quantities are held constant.

Chimere has been used for many case studies (see [Chimere Documentation] for examples) and is producing forecast for France and Europa (see e.g. `www.lmd.polytechnique.fr/mm5`). It is in development since 1997 and still newer versions are produced.

3 The Atmospheric Boundary Layer

Two important parameters for calculating surface concentrations are the boundary layer height and the vertical diffusion coefficient (K_z). In the model the boundary layer height bounds the vertical extent in which turbulent diffusion is taken into account so it effectively limits the vertical dispersion of pollutants. The turbulence parameter K_z defines the rate at which pollutants are vertically dispersed thus low values trap the pollutants near the surface. Since it is to be determined whether these parameters are modelled correctly, a summary of their calculation is outlined in this chapter. Furthermore the parameterizations which are used by ECMWF and Chimere to calculate the boundary layer height are introduced.

3.1 General Aspects of the Atmospheric Boundary Layer

The atmospheric boundary layer (ABL) is the lowest part of the atmosphere which is in direct contact with the surface of the earth. The thickness of this layer can be defined as that part of the atmosphere which is directly influenced by the presence of the earth's surface and responds to surface forcings with a timescale of less than an hour [Stull, 1988]. Surface forcings are e.g. a temperature flux, moisture flux, emissions etc.

In general the ABL is turbulent. A dimensionless number indicating the turbulence intensity is the Reynolds number. It can be defined as $Re \equiv Uh/\nu$ with U the speed just above the boundary layer, h the height of the boundary layer and ν the kinematic viscosity. For a boundary layer of $1000\,m$ high, a geostrophic wind (wind just above the boundary layer) of $5\,m/s$ the Reynolds number is $Re \approx 10^8$. Flow over a flat smooth plate starts to become turbulent at $Re \approx 10^4$ when for h the thickness of the laminar boundary layer at the point of becoming turbulent is used. However, in an atmospheric boundary layer the turbulence is suppressed if the thermal radiative flux is negative (i.e. away from the surface), then transition to turbulence is delayed.

There are two sources of turbulence; wind shear and thermal convection. The first is due to shear instability, the second due to thermal instability creating thermals of about the size of the ABL depth. The latter instability is due to a positive radiative flux (i.e. to the ground). This flux can also change sign causing turbulence to be suppressed rather than created.

These turbulence sources cause a range of different ABL structures ranging from free convection (only thermal convection), through forced convection (thermal convection and wind shear), neutral conditions (only wind shear) and stable boundary layers to very stable boundary layers. In the latter two cases turbulence is suppressed (the boundary layer is stable) and in the last case also the wind velocity is low (geostrophic winds lower than about $5\,m/s$). In that case the turbulence can show intermittent behavior.

During fair weather over land the daily cycle of the sun causes a diurnal variation of heating and cooling of the earth's surface. This affects the air directly above the surface and causes a diurnal cycle in the ABL structure as well, this is shown in figure 3.1. During the day the earth is warmed by the sun and causes thermals (rising columns of air) to develop. These thermals cause vigorous mixing of mass, momentum, energy, trace gases and aerosols throughout the whole boundary layer depth. This is why it is also called a

mixing layer. At the top of the mixing layer air is entrained from the free atmosphere, this is the entrainment zone (EZ). Following sunset the surface cools and thermals cease to exist. The air directly above the surface cools and a stable boundary layer starts to form. The remainder of the former mixing layer that is above the stable boundary layer is called a residual layer which has neutral stability. It is bounded at the top by a capping inversion, this temperature inversion (where temperature increases with height rather than decreases) 'caps' the residual layer and there is no exchange with the free atmosphere. After sunrise thermals start to develop again. At first the mixing layer grows rather slowly because the heat is confined to warming the cooled air in the stable boundary layer. When it reaches the residual layer, the thermals rise rapidly to the capping inversion. This causes a very rapid rise of the mixing layer height. After this, the mixing layer height increases slowly again.

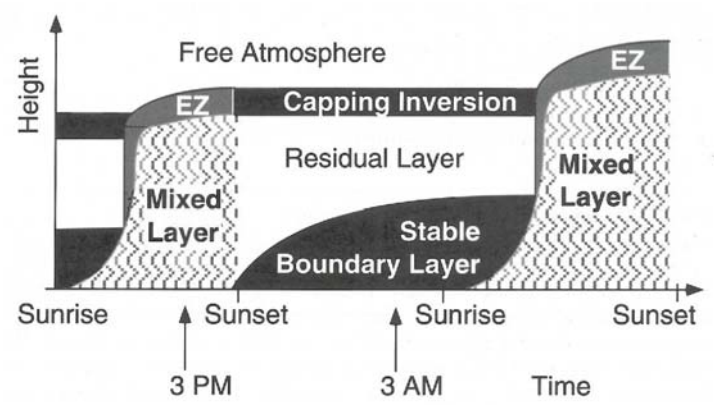

Figure 3.1: A typical diurnal cycle of the ABL, copied from [Holtslag et al. (1998)] pg. 23. EZ stands for Entrainment Zone.

In vertical direction four regions can be identified, the upper three are plotted in figure 3.2. Ultimately the presence of the earth's surface is felt through molecular processes in the first layer; the viscous sublayer. This layer is only a few millimeters thick and only here viscosity is important.

The roughness layer is the second layer closest to the ground. Its thickness depends on the roughness but can be in the range of a few tens of centimeters for grasslands to a few tens of meters for a forest or an urban area. The earth's surface is in general aerodynamically rough. This means that the roughness elements have a rather large influence on the development of turbulence and the wind profiles.

The third layer is the surface layer. This is in general defined as the lowest 10% of the ABL height. Here the velocity varies approximately logarithmically in a mixed layer. In a stable boundary layer this layer is not well defined.

The highest layer is the outer or Ekman layer. Here the velocity is almost constant in a mixed layer. Often there is a temperature inversion at the top of the ABL above which the free atmosphere is located. The free atmosphere is in general free of turbulence.

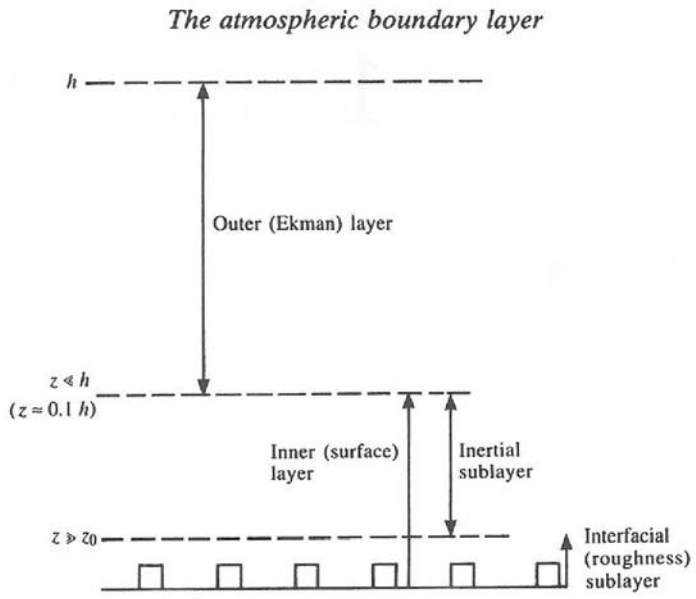

Figure 3.2: The layers as identified within an atmospheric boundary layer. z is the vertical coordinate, h is the boundary layer height and z_0 is the surface roughness. Copied from [Garratt (1992)]

3.2 Potential temperature

The potential temperature of an air parcel is that temperature which it would aquire when it would be taken to the surface adiabatically. This means that an atmosphere with a uniform entropy would have a constant potential temperature. The gradient of the potential temperature is an important parameter for thermal stability.

The relations between potential temperature and normal temperature can be derived as follows. Start with the isentropic relations for a calorically perfect gas:

$$\frac{T_1}{T_2} = \left(\frac{p_1}{p_2}\right)^{(\gamma-1)/\gamma}$$

With $\gamma \equiv C_p/C_v$ with C_p the specific heat at constant pressure and C_v the specific heat at constant volume. State 1 is the state of the air parcel considered. Now take for state 2 the state at the surface, so $p_2 = p_0$ and $T_2 = \theta$, and θ being the potential temperature. In this way the relation between potential and normal temperature becomes:

$$\theta = T\left(\frac{p}{p_0}\right)^{(1-\gamma)/\gamma} \tag{3.1}$$

3.3 Thermal Stability

Thermal stability is an important parameter in the ABL, because it determines whether thermals form or not. Thermals have a large influence on vertical mixing. To determine the stability of the ABL the gradient of the potential temperature (θ) is needed.

To understand the relation between θ and the stability of the ABL an air parcel is followed which rises adiabatically and reversibly from its original position (thus with constant entropy, note θ of the parcel does not change). Because of the decrease in pressure, the parcel will expand. It is clear the parcel will be forced back if the density of the surroundings is smaller than the density of the parcel. If the density of the surroundings varies such that the entropy does not change with height, the parcel will always find itself surrounded by air of the same density. This means that a neutral atmosphere is an atmosphere with uniform entropy, and thus with constant virtual potential temperature.

Thus the atmosphere is statically stable when with increasing height the density decreases faster than in an adiabatic atmosphere. To decrease the density, the temperature should increase, so the next stability criteria can be derived:

$$\begin{aligned} \frac{d\theta}{dz} &> 0, \text{ (stable)} \\ \frac{d\theta}{dz} &= 0, \text{ (neutral)} \\ \frac{d\theta}{dz} &< 0, \text{ (unstable)} \end{aligned}$$

3.4 Flow description

The complete set of equations governing the flow in an ABL consists of six partial differential equations. The momentum equations (i.e. the Navier-Stokes equations), the continuity equation, the energy equation and the humidity equation (which expresses the conservation of water vapor). The system is closed by two equations of state for a calorically perfect gas.

No cloud forming is taken into account in this report so the specific humidity q never reaches its saturation point. Humid air does have a different density but this can be accounted for when the virtual potential temperature is used (see [Stull, (1988)] appendix D for a derivation). This is the potential temperature dry air would have when at the same density as humid air. This means the humidity equation can be left out of this report.

For the flow these general assumptions can be made:

- The gas is a Newtonian fluid.
- The gas is assumed to be calorically perfect, which is to say it obeys the gas law ($p = \rho RT$, with p pressure, ρ density, R the specific gas constant for dry air and T the temperature) and the specific heat at constant pressure and volume are constant (C_p and C_v respectively). Furthermore the internal energy $e = C_v T$ with T the temperature in degrees Kelvin.
- The dynamic viscosity μ is assumed to be constant
- The dissipation due to viscous stresses is neglected in the energy equation.

- Deviations of the fluid properties (i.e. pressure p, temperature T, density ρ, potential temperature θ) from the reference state are small, i.e. p^*/p_0, T^*/T_0, ρ^*/ρ_0 and θ^*/θ_0 are all $\ll 1$. The asterisk denotes a deviation from the reference state. The reference state can be chosen.
- Density changes resulting from pressure changes are negligible (first part of the Boussinesq approximation, this is an approximation valid for the lowest few kilometers of the earth's atmosphere and consists of two parts, see e.g. [Spiegel and Veronis, (1959)], [Garratt, (1992) section 2.2] or section 3.4.5).
- Density changes resulting from temperature changes are important only as they directly affect buoyancy (second part of the Boussinesq approximation).

3.4.1 Coordinate System

First the coordinate system is defined. The coordinate system is attached to the earth's surface with the y-axis positive in Northern direction, the x-axis positive in Eastern direction and the z axis positive upwards, see figure 3.3. This means:

$$\begin{aligned} x &= \lambda|\mathbf{r}|\cos\phi \\ y &= |\mathbf{r}|\,\phi \\ z &= |\mathbf{r}| - a \end{aligned}$$

These are spherical coordinates with $\phi = \phi_r - \phi_0$, $\lambda = \lambda_r - \lambda_0$ and (ϕ_r,λ_r) the latitude and longitude of $\mathbf{r}$ (the location vector of a point in the coordinate system) and (ϕ_0,λ_0) the latitude and longitude of the origin of the coordinate system. The coordinate system has a non-inertial frame of reference and this introduces extra body forces in the momentum equations.

3.4.2 Momentum equation

It can be deduced that the momentum equations in a spherical coordinate system rotating at angular speed Ω become (see for example [Holton, (1972)]):

$$\frac{Du}{Dt} - \frac{uv\tan\phi}{a} + \frac{uw}{a} = -\frac{1}{\rho}\frac{\partial p}{\partial x} + 2\Omega v\sin\phi - 2\Omega w cos\phi + F_{rx} \qquad (3.2)$$

$$\frac{Dv}{Dt} + \frac{u^2\tan\phi}{a} + \frac{vw}{a} = -\frac{1}{\rho}\frac{\partial p}{\partial y} - 2\Omega u\sin\phi + F_{ry} \qquad (3.3)$$

$$\frac{Dw}{Dt} - \frac{u^2+v^2}{a} = -\frac{1}{\rho}\frac{\partial p}{\partial z} - g + 2\Omega u\cos\phi + F_{rz} \qquad (3.4)$$

In these equations $D/Dt = \partial/\partial t + u\partial/\partial x + v\partial/\partial y + w\partial/\partial z$ is the material or total derivative. Furthermore a is the radius of the earth and F_{ri} are the friction terms. Also

$$u \equiv |\mathbf{r}|\cos\phi\frac{D\lambda}{Dt} = \frac{Dx}{Dt}, \qquad v \equiv |\mathbf{r}|\frac{D\phi}{Dt} = \frac{Dy}{Dt}, \qquad w \equiv \frac{Dz}{Dt}$$

are the definitions of the different velocities. The only approximation in the equations (3.2)-(3.4) is that $|r|$ is replaced by a, this is because $|r| = a + z \approx a$.

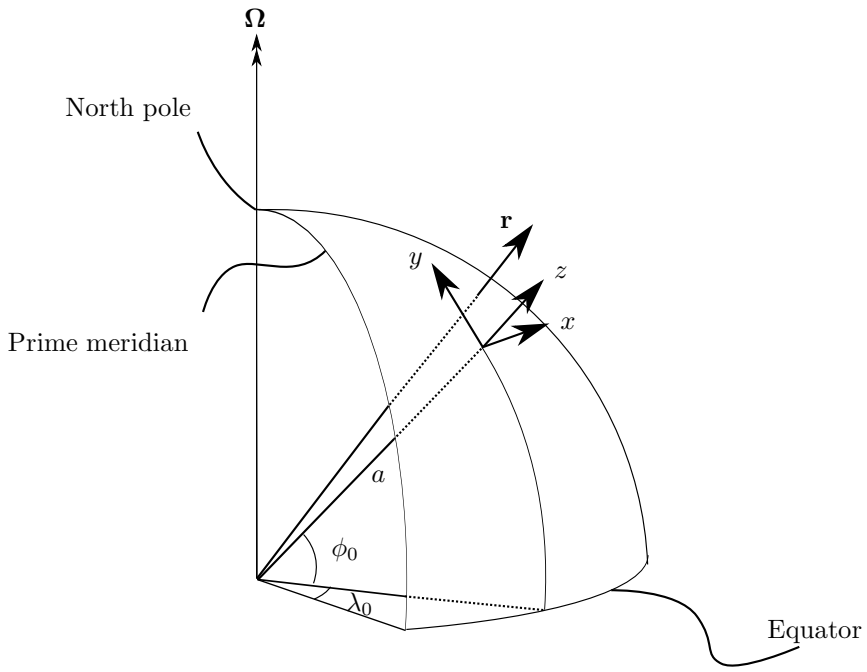

Figure 3.3: The coordinate system as used throughout this report. x and y are the surface coordinate directions, $\mathbf{\Omega}$ is the rotation vector, $\mathbf{r}$ is the location vector of a point in the coordinate system, ϕ_0 is the latitude and λ_0 is the longitude of the origin of the x-y coordinate system.

By doing this, it can be shown, according to [Holton, (1972)], that the terms proportional to $\cos\phi$ must be neglected if the equations are to satisfy angular momentum conservation.

The equations can be further simplified. For mid-latitude ($\phi \approx 45°$) synoptic-scale motions, the next scales of the field variables based on observed values can be defined (from [Holton, (1972)]):

U	$\sim$	$10\ m\ s^{-1}$	horizontal velocity scale
W	$\sim$	$1\ cm\ s^{-1}$	vertical velocity scale
L	$\sim$	$10^6\ m$	length scale
H	$\sim$	$10^4\ m$	depth scale
$\delta P/\rho$	$\sim$	$10^3\ m^2\ s^{-2}$	horizontal pressure fluctuation scale
L/U	$\sim$	$10^5\ s$	time scale

From these orders of magnitude of the different terms in eqs. (3.2)-(3.4) can be estimated as shown in table 3.1. It can be seen that term B and F are approximately in balance. This is the geostrophic approximation

$$(u_g, v_g) = \frac{1}{f\rho}\left(\frac{\partial p}{\partial x}, -\frac{\partial p}{\partial y}\right) \tag{3.5}$$

with (u_g, v_g) the geostrophic wind components and $f = 2\Omega sin\phi$ the Coriolis parameter. Outside the boundary layer and away from the tropic region the velocity field is in approximate geostrophic balance with the pressure field.

	A	B	C	D	E	F	G
$x-$ Eq.	$\frac{Du}{Dt}$	$-2\Omega v\sin\phi$	$+2\Omega w\cos\phi$	$+\frac{uw}{a}$	$-\frac{uv\tan\phi}{a}$	$=-\frac{1}{\rho}\frac{\partial p}{\partial x}$	$+F_{rx}$
$y-$ Eq.	$\frac{Dv}{Dt}$	$+2\Omega u\sin\phi$		$+\frac{vw}{a}$	$-\frac{u^2\tan\phi}{a}$	$=-\frac{1}{\rho}\frac{\partial p}{\partial x}$	$+F_{ry}$
Scales	U^2/L	f_0U	f_0W	$\frac{UW}{a}$	$\frac{U^2}{a}$	$\frac{\delta P}{\rho L}$	$\frac{\nu U}{H^2}$
$(m\ s^{-2})$	10^{-4}	10^{-3}	10^{-6}	10^{-8}	10^{-5}	10^{-3}	10^{-12}

Table 3.1: Scale analysis of the horizontal momentum equations, after [Holton, (1972)]

From the table it is also clear that the 'curvature terms' (terms D and E) are usually negligible. Except maybe near the poles (where $|\tan\phi|\to\infty$). However, for the most Northern part of the AMFIC domain $\tan 52^\circ \approx 1$ so these terms can be neglected.

The influence from friction (term G) apparently is entirely negligible. However, its influence is more indirect outside the viscous sub-layer. The viscous sub-layer is the layer where the friction term dominates the forcings in the momentum equations, but its thickness is in the order of a millimeter and therefore not relevant in the boundary layer equations.

Viscosity causes the velocity to vanish at the wall and thus imposes the no-slip boundary condition. As a consequence even for fairly weak winds the velocity gradients (shear) become large near the wall which causes turbulence to be produced. Turbulence causes the transport of heat, moisture and momentum in the vertical direction at a rate much faster than can be achieved by molecular processes only. Certainly the latter has a great influence on the vertical velocity profile and is the main source of the deviation from the geostrophic balance. This means that the horizontal momentum equations become

$$\frac{Du}{Dt} = -\frac{1}{\rho}\frac{\partial p}{\partial x} + fv + F_{rx} \tag{3.6}$$

$$\frac{Dv}{Dt} = -\frac{1}{\rho}\frac{\partial p}{\partial y} - fu + F_{ry} \tag{3.7}$$

The order of magnitude of the terms in the vertical momentum equation are shown in table 3.2. This shows that to a very good approximation the vertical pressure distribution is in balance with the gravitational force. This is the hydrostatic approximation:

$$\frac{1}{\rho}\frac{\mathrm{d}p}{\mathrm{d}z} = -g \tag{3.8}$$

$z-$ Eq.	Dw/Dt	$-2\Omega u\cos\phi$	$-(u^2+v^2)/a$	$=-\rho^{-1}\partial p/\partial z$	$-g$	$+F_{rz}$
Scales	UW/L	f_0U	U^2/a	$P_0/(\rho H)$	g	νWH^{-2}
$(m\ s^{-2})$	10^{-7}	10^{-3}	10^{-5}	10	10	10^{-15}

Table 3.2: Scale analysis of the vertical momentum equation, after [Holton, (1972)]

This also means that the vertical velocity cannot be determined from the vertical momentum equation [Holton, (1972)]. This can be done indirectly by considering horizontal convergence or divergence and applying mass conservation.

3.4.3 Continuity equation

The continuity equation in Cartesian coordinates is:

$$\frac{1}{\rho}\frac{D\rho}{Dt}+\nabla\cdot\mathbf{u}=0 \tag{3.9}$$

The length and time scales of a boundary layer are such that the curvature of the earth is negligible. This means the formulation in the Cartesian coordinates approaches the formulation in the spherical coordinates. Furthermore, the rotation of the coordinate system does not appear in this equation. This means that the formulation in Cartesian coordinates approximates the formulation in spherical coordinates.

3.4.4 Energy equation

The energy equation in spherical coordinates can be derived (see e.g. [Holton, (1972)]) to be:

$$C_v\frac{DT}{Dt}+p\frac{D\alpha}{Dt}=J \tag{3.10}$$

With $\alpha\equiv 1/\rho$ and J is the source term. The Coriolis force, $-2\mathbf{\Omega}\times\mathbf{U}$, cannot perform work since it always acts perpendicular to the velocity vector so it does not appear in this equation.

3.4.5 Boussinesq approximation

The horizontal momentum equations (eqs. (3.6)-(3.7)) and the continuity equation (3.9) can be further simplified. This can be done by writing the pressure and density as a sum of the reference state and a deviation from this state: $p=p_0(z)+p^*(x,y,z)$ and $\rho=\rho_0(z)+\rho^*(x,y,z)$. The reference pressure and density (p_0 and ρ_0) are assumed to satisfy the hydrostatic equation *exactly*:

$$\frac{\mathrm{d}p_0}{\mathrm{d}z}\equiv-\rho_0 g$$

and the deviations to this basic state (ρ^* and p^*) are assumed to be small compared to this basic state (see section 3.4). For ease of derivation, write the momentum equation in vector form

$$\rho\frac{D\mathbf{u}}{Dt} = -\nabla p + \rho\mathbf{f}_u + \rho\mathbf{g} + \rho\mathbf{F}_r$$

Where $\mathbf{f}_u \equiv (fv, -fu)$. Now, substitute the decomposed pressure and density, and divide by ρ_0

$$\left\{1+\frac{\rho^*}{\rho_0}\right\}\frac{D\mathbf{u}}{Dt} = -\frac{1}{\rho_0}\nabla p^* + \left\{1+\frac{\rho^*}{\rho_0}\right\}\mathbf{f}_u + \frac{\rho^*}{\rho_0}\mathbf{g} + \left\{1+\frac{\rho^*}{\rho_0}\right\}\mathbf{F}_r + \left[-\rho_0^{-1}\frac{\mathrm{d}p_0}{\mathrm{d}z} + g\right]$$

where the term inside the square brackets is identically zero. The term between curly brackets are ≈ 1. The buoyancy term ($\rho^*\mathbf{g}/\rho_0$) cannot be neglected, it is the density fluctuations that drive the convective motion when the surface is heated. This is the second part of the Boussinesq approximation. Thus the horizontal momentum equations can be written as (dropping the asterisk):

$$\frac{Du}{Dt} = -\frac{1}{\rho_0}\frac{\partial p}{\partial x} + fv + F_{rx} \tag{3.11}$$

$$\frac{Dv}{Dt} = -\frac{1}{\rho_0}\frac{\partial p}{\partial y} - fu + F_{ry} \tag{3.12}$$

The continuity equation (3.9) can be simplified by noting that the velocity of the flow is much smaller than the speed of sound and thus the flow can be regarded as incompressible, this is the first part of the Boussinesq equation. Thus the incompressible variant of the continuity equation survives:

$$\nabla \cdot \mathbf{u} = 0 \tag{3.13}$$

3.5 Turbulence

If the Reynolds number of a flow is high enough, or in the presence of convection, turbulent eddies form. The size of these eddies ranges from the size of the flow problem, in this case the boundary layer height of $1\,km$ say, to the size at which the eddies dissipate due to viscosity, usually about $1\,mm$ (which is the Kolmogorov scale). Since it is impossible to resolve all the scales with the currently available computing power, a different approach has to be undertaken to solve the horizontal momentum equations 3.11 and 3.12. Here the Reynolds averaging method is used which is introduced in the next section. This leads to a closure problem which is solved with the flux–gradient theory and similarity theory.

3.5.1 Reynolds Averaging Method

The Reynolds averaging method consist of two parts. First all field variables are written as a sum of a time averaged part ($\bar{\psi} \equiv 1/\Delta t \int \psi \mathrm{d}t$, with ψ a field variable) and a perturbation ($1/\Delta t \int \psi' \mathrm{d}t \equiv 0$), thus

$$\begin{aligned}
\mathbf{u}(\mathbf{x},t) &= \bar{\mathbf{u}}(\mathbf{x},t) + \mathbf{u}'(\mathbf{x},t) \\
p(\mathbf{x},t) &= \bar{p}(\mathbf{x},t) + p'(\mathbf{x},t) \\
\rho(\mathbf{x},t) &= \bar{\rho}(\mathbf{x},t) + \rho'(\mathbf{x},t) \\
\theta(\mathbf{x},t) &= \bar{\theta}(\mathbf{x},t) + \theta'(\mathbf{x},t)
\end{aligned}$$

where the bar denotes the variable is time averaged and the prime denotes the fluctuation. The period over which time averaging takes place is much larger than the time scale of turbulent fluctuations but small enough to assume the mean flow to be constant. This is the Reynolds decomposition. These are substituted in eqs. 3.11 and 3.12. Then the whole equations are averaged, leading to:

$$\frac{\bar{D}\bar{u}}{Dt} = -\frac{1}{\rho_0}\frac{\partial \bar{p}}{\partial x} + f\bar{v} - \left[\frac{\partial \overline{u'u'}}{\partial x} + \frac{\partial \overline{u'v'}}{\partial y} + \frac{\partial \overline{u'w'}}{\partial z}\right] + \bar{F}_{rx}$$

$$\frac{\bar{D}\bar{v}}{Dt} = -\frac{1}{\rho_0}\frac{\partial \bar{p}}{\partial y} - f\bar{u} - \left[\frac{\partial \overline{u'v'}}{\partial x} + \frac{\partial \overline{v'v'}}{\partial y} + \frac{\partial \overline{v'w'}}{\partial z}\right] + \bar{F}_{ry}$$

With $\bar{D}/Dt \equiv \partial/\partial t + \bar{\mathbf{u}} \cdot \nabla$, this gives the change of a variable when traveling with the *mean* flow.

Away from regions with horizontal inhomogeneities (e.g. shorelines, urban areas or forest edges) the equations can be simplified by assuming horizontal homogeneity. This means the horizontal derivatives of the terms in square brackets can be neglected. Furthermore, when outside the viscous sublayer the friction terms can also be neglected. And in section 3.4.2 it has been shown that, to a first approximation, the inertial acceleration terms can be neglected. This lead to the geostrophic balance (eq. 3.5). All this gives the approximate boundary layer equations:

$$f(\bar{v} - \bar{v}_g) - \frac{\partial \overline{u'w'}}{\partial z} = 0 \tag{3.14}$$

$$-f(\bar{u} - \bar{u}_g) - \frac{\partial \overline{v'w'}}{\partial z} = 0 \tag{3.15}$$

The terms $\overline{u'w'}$ and $\overline{v'w'}$ are covariances between the fluctuating parts of the variables. u_g and v_g are the velocity components of the geostrophic balance defined in 3.5. The covariance terms are extra terms arising from averaging the momentum equations. They can be interpreted as fluxes (see figure 3.4). When air parcel (B) moves downwards in figure 3.4a it carries the local value of horizontal speed with it before mixing in the lower surroundings. This means a positive momentum perturbation is transported downwards meaning there is a negative momentum flux. Thus positive gradient means a negative flux and visa versa. Air parcels can also carry other fluid properties like potential temperature and humidity, this means these quantities are transported as well when a gradient exists. Some definitions can be given:

$$\text{Vertical Momentum Flux :} \quad \tau \equiv \rho[\overline{u'w'}^2 + \overline{v'w'}^2]^{1/2} \tag{3.16}$$

$$\text{Sensible Heat Flux :} \quad H \equiv \rho C_p \overline{w'\theta'} \tag{3.17}$$

$$\text{Latent Heat Flux :} \quad L_H \equiv \rho\lambda \overline{w'q'} \tag{3.18}$$

where λ is the latent heat of vaporization of water and q the specific humidity. The vertical momentum fluxes have the same effect as viscous stresses (i.e. momentum transport and dissipation), that is why they are called Reynolds stresses. Their value is usually some orders of magnitudes larger than the viscous stress in high Reynolds number flows.

The sensible heat flux is the flux of air temperature in the boundary layer, it is positive (upward) when the surface is heated by the sun which on its turn

heats the air above. It can become negative when the surface cools at night due to radiation losses, in that case the surface cools the air directly above it. The sign of the sensible heat flux is also an indicator for thermal stability. When positive the potential temperature gradient is negative through equation 3.21, indicating an unstable boundary layer, and visa versa.

The latent heat flux is the flux of latent energy stored in water vapor. Evaluated near the surface it is the amount of energy used to evaporate water from the surface.

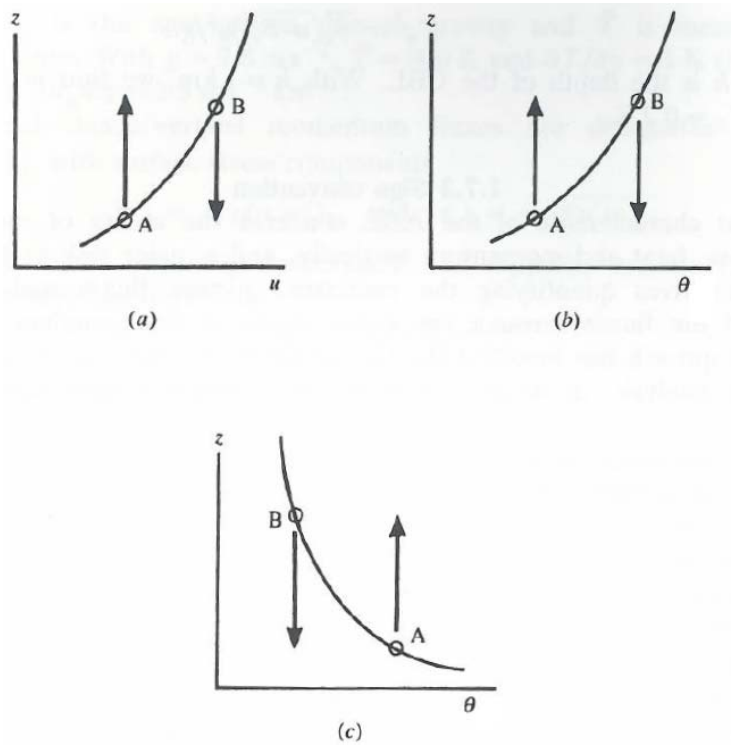

Figure 3.4: Schematic representation of typical near-surface profiles of (a) wind speed, (b) potential temperature in stable conditions and (c) potential temperature in unstable conditions. The air parcels designated A (B) have positive (negative) vertical velocity fluctuation w' and carry negative (positive) property fluctuations u' and θ' in (a) and (b), and positive (negative) fluctuations in (c). By convention, the covariances $u'w'$ and $w'\theta'$ in (a) and (b) are negative (fluxes downwards), and in (c) are positive (fluxes upwards). Copied from [Garratt, (1992)].

3.5.2 The Flux–Gradient Theory

Analytical solutions of equations 3.14 and 3.15 are generally not possible. This is because the Reynolds stresses arising from averaging the momentum equations are extra unknowns for which expressions cannot be derived. This is the turbulent closure problem. One approach to close the equations is to assume that turbulent eddies act in a manner analogous to molecular diffusion so that the flux of a given field is proportional to the local gradient of the mean. In this

case the Reynolds stresses in equations 3.14 and 3.15 and the temperature flux $\overline{w'\theta'}$ can be written as

$$\overline{u'w'} = -K_z \left(\frac{\partial \bar{u}}{\partial z} \right) \tag{3.19}$$

$$\overline{v'w'} = -K_z \left(\frac{\partial \bar{v}}{\partial z} \right) \tag{3.20}$$

$$\overline{w'\theta'} = -K_h \left(\frac{\partial \bar{\theta}}{\partial z} \right) \tag{3.21}$$

where K_z is the so-called vertical diffusion coefficient (or eddy viscosity) and K_h the eddy diffusivity of heat. This closure scheme is called K–theory. Note that K_z and K_h are a property of the flow rather than the fluid, like viscosity is. This means that the value of K_z depends on e.g. stability, surface roughness and wind shear.

When using K–theory and assuming K_z is constant, equations 3.14 and 3.15 do have an analytic solution called the Ekman spiral. However, this is only valid for neutral cases and its height is still dependent on the exact value of K_z. Furthermore, this solution is hardly, if ever, observed in reality.

3.5.3 Similarity Theory

There are several processes which influence turbulence in the boundary layer. Examples are wind shear, the sensible heat flux, the potential temperature profile and surface roughness. Similarity theory uses dimensional analysis to find expressions used for scaling. If turbulence generation is dominated by only a few physical processes, characteristic quantities of these processes can be combined in an expression and used for scaling of field variables.

For example the consequence of the no-slip boundary condition is a velocity gradient in the boundary layer. This can be characterized by τ_s which is eq. 3.16 evaluated near the surface. This can be be divided through by ρ, defining the friction velocity:

$$u_* \equiv \sqrt{\frac{\tau_s}{\rho}} = \left[(\overline{u'w'})_s^2 + (\overline{v'w'})_s^2 \right]^{1/4}, \qquad [m/s] \tag{3.22}$$

Where the subscript s denotes near surface values. This can be used to characterize turbulence due to wind shear.

An other way to create turbulence is due to buoyancy. This is related to air parcels under gravity forces induced by the surface sensible heat flux H_s (eq. 3.17 evaluated near the surface). But rather than H_s, $(\overline{w'\theta'})_s$ is used and scaled with u_* to define a temperature scale $\theta_* = -(\overline{w'\theta'})_s / u_*$. With this the Obukhov length scale can be defined:

$$L \equiv \frac{u_*^2}{k \frac{g}{T_s} \theta_*}, \qquad [m] \tag{3.23}$$

Here T_s is the temperature at the surface and k is the von-Kármán constant equal to 0.4. The Obukhov length can be interpreted as the height above the surface where buoyancy production starts to dominate over shear production. This can be used with h, the boundary layer height, to create a parameter,

h/L indicating the stability of the boundary layer. A positive h/L means H_s is negative indicating stable conditions. When $|h/L|$ is small, the boundary layer is close to neutral and $-h/L \to \infty$ means free convection is approached.

Another scale relating to the buoyancy is the convective velocity scale:

$$w_* \equiv \left[\frac{gh}{\theta}\left(\overline{w'\theta'}\right)_s\right]^{1/3}, \qquad [m/s] \tag{3.24}$$

This is a measure for the intensity of convection in the boundary layer. It is of the same order of magnitude as the velocity fluctuation induced by thermals.

The last parameter to be introduced here is the flux Richardson number, Rf. Change in the turbulent kinetic energy $e = (u'^2 + v'^2 + w'^2)/2$ is due to mechanical (shear) production

$$MP \equiv -\overline{u'w'}\partial\bar{u}/\partial z - \overline{v'w'}\partial\bar{v}/\partial z,$$

buoyant production or loss

$$BPL \equiv \overline{w'\theta'}(g/\bar{\theta}),$$

terms for redistributing e by pressure and transport and a dissipative term. The flux Richardson number is defined as $Rf = -BPL/MP$, thus:

$$Rf \equiv \frac{\overline{w'\theta'}(g/\theta_s)}{\overline{u'w'}\partial\bar{u}/\partial z + \overline{v'w'}\partial\bar{v}/\partial z} \tag{3.25}$$

The flux Richardson number is a local measure of turbulence intensity. When $Rf < 0$, implying $\overline{w'\theta'} > 0$, turbulence is sustained by convection. Observations suggest that only when Rf is less than about 0.25 (i.e., mechanical production exceeds buoyancy damping by a factor of 4) the mechanical production is intense enough to sustain turbulence. Perturbation theory confirms this number for the gradient Richardson number defined in eq. 3.27, see e.g. [Kundu and Cohen, (2004)] chapter 12 paragraph 7.

Above quantities are used to calculate K_z and the boundary layer height in Chimere and ECMWF as will be shown in the next section.

3.6 Parameterizations used by Chimere and ECMWF

3.6.1 Vertical Diffusion Coefficient

To calculate K_z Chimere uses a parameterization following [Troen and Mahrt, (1986)]:

$$K_z = k w_s z \left(1 - \frac{z}{h}\right)^{1/3} \tag{3.26}$$

where k is the von-Kármán constant and w_s is a vertical scale given by similarity formulae:

- In the stable case ($L > 0$): $w_s = u_*/(1 + 4.7z/L)$
- in the unstable case ($L < 0$): $w_s = (u_*^3 + 2.8ew_*^3)^{1/3}$

Where $e = \max(0.1, z/h)$, L the Obukhov length (eq. 3.23), w_* the convective velocity scale (eq. 3.24, u_* the friction velocity (eq. 3.22) and h the boundary layer height. Thus there is a profile which is observed by measurements, $z(1 - z/h)^{1/3}$, which is scaled by w_s. A minimum value for K_z of $0.1\,m^2/s$ is assumed. To calculate K_z, the next variables are needed for input:

- The potential temperature profile $\bar{\theta}(z)$
- The sensible heat flux H
- The wind profile $\bar{\mathbf{u}}(z)$
- The surface roughness z_0
- The boundary layer height h

3.6.2 Boundary Layer Height Calculation

Both ECMWF and Chimere use for their calculation of the boundary layer height the formulation introduced in [Troen and Mahrt, (1986)] but there are differences. The whole calculation is tedious and will not be detailed here. Only an overview of the important ideas is given.

Both ECMWF and Chimere seek the height at which the Richardson number reaches a critical value. However, the flux Richardson number is a local parameter and thus dependent on local gradients. When a profile is discretized, the gradients of a variable can become very sensitive to small changes of that variable. This is why the bulk Richardson number (Ri_B) is used instead. For its derivation first the gradient Richardson number (Ri) is obtained by substituting eqs. 3.19–3.21 in eq. 3.25:

$$Ri = \frac{(g/\bar{\theta})\partial\bar{\theta}/\partial z}{[(\partial\bar{u}/\partial z)^2 + (\partial\bar{v}/\partial z)^2]} \tag{3.27}$$

Thus $Ri = K_z/K_h Rf$, $K_z/K_h \equiv Pr$ is called the turbulent Prandtl number. Now approximate $\partial\bar{\theta}/\partial z$ as $\Delta_h\bar{\theta}/\Delta_h z$ and approximate $\partial\bar{u}/\partial z$ and $\partial\bar{v}/\partial z$ as $\Delta_h\bar{u}/\Delta_h z$ and $\Delta_h\bar{v}/\Delta_h z$, respectively. The Δ_h denotes the difference between surface values and the values at the boundary layer height. Since the surface values of the velocity is zero and $\Delta_h z = h$ the bulk Richardson number reduces to:

$$Ri_B = \frac{hg(\bar{\theta}(h) - \bar{\theta}_s)}{\bar{\theta}(h)(\bar{u}^2(h) + \bar{v}^2(h))} \tag{3.28}$$

This relation thus uses the approximate gradients of the flow. The critical value of 0.25 only applies for local gradients. The bulk Richardson number averages out large gradients, thus a higher critical value is needed. [Troen and Mahrt, (1986)] proposed 0.5, which is used by Chimere.

For the sake of completeness it is noted that during day time when a mixing layer exist, the thermal plumes make K–theory invalid. This is because thermals mix air over the whole boundary layer height which smoothes the profile of $\bar{\theta}$ and make it close to neutral, suggesting near zero sensible heat flux (see eq. 3.21 and 3.17). But the mixing layer exists because of a large sensible heat flux. Thus a different parameterization scheme is needed in these cases. This

involves calculating the height a parcel which is heated at the surface would reach. Both Chimere and ECMWF incorporate this effect differently but the details on the calculation are not given here. This is because our interest is mainly in nocturnal boundary layers. To calculate the boundary layer height, the next variables are needed for input:

- The potential temperature profile $\bar{\theta}(z)$
- The wind profile $\bar{\mathbf{u}}(z)$

3.6.3 Friction Velocity

The friction velocity (u_*) is used to calculate the boundary layer height and the vertical diffusion coefficient, it needs to be parameterized. Since u_* is a measure for the shear stress (see eq. 3.22), it is expected to be in the form of a drag law. A drag law relates known variables to the surface stress. In Chimere it is of the form:

$$u_* = C_d\sqrt{|\bar{\mathbf{u}}_{10}|^2 + (1.2w_*)^2}$$

With $\bar{\mathbf{u}}_{10}$ the wind vector at $10\,m$ and C_d a non dimensional drag coefficient. It has the form:

$$\begin{aligned} C_d &= C_{d,n}\sqrt{f} \\ C_{d,n} &= k/\ln(10/z_0) \end{aligned}$$

With $C_{d,n}$ the drag coefficient for the neutral case ($Ri = 0$), k the Von Karman constant (0.4), z_0 the roughness length and f a correction term for non-neutral cases, it has the next properties:

$$\begin{aligned} f(Ri_l = 0) &= 1 \\ \text{Unstable case } (Ri < 0): \quad f &\sim \sqrt{|Ri_l|}, \qquad \text{range: } [1, \infty\rangle\,, \quad f = f(Ri, z_0) \\ \text{Stable case } (Ri > 0): \quad f &\sim \frac{1}{\sqrt{|Ri_l|}}, \qquad \text{range: } \langle 0, 1]\,, \quad f = f(Ri) \end{aligned}$$

Where Ri_l is the Richardson number evaluated at the lowest grid level and z_0 is the surface roughness. The exact expression for f is tedious and will not be given here. To calculate the friction velocity, the next variables are needed for input:

- The potential temperature at the lowest grid level $\bar{\theta}(0)$
- The sensible heat flux H
- The wind at $10\,m$ $\bar{\mathbf{u}}_{10}$
- The surface roughness z_0

The details of calculating the boundary layer and the vertical diffusion coefficient are outlined and their dependencies are given. This gives a better understanding in which parameters influence vertical dispersion in the boundary layer height in Chimere.

For more details about the theory presented in this chapter see e.g. [Stull, (1988)], [Garratt, (1992)], [Holtslag et al., (1998)] (on boundary layer theory), [Holton, (1972)] (on dynamic meteorology), [Kundu and Cohen, (2004)] (on general fluid dynamics) and [Pope, (2000)] (on turbulence).

4 Sensitivity Studies

In this chapter several parameters of Chimere will be varied to study their influence on the model output. For this different simulations have been carried out and results are compared with the standard simulation. The standard simulation is the simulation carried out with the settings as used currently in the operational forecasts of air quality over China as used in the EU project AMFIC (see `www.amfic.eu/bulletin`). The settings for the standard simulation are:

Parameter	**Setting**
Grid size	0.25° in each direction
Number of vertical layers	8
Physical time step / Chemical time step	10/10 min
Minimal value of K_z	$0.1\,m^2/s$
Minimal value of the boundary layer height	$20\,m$
Domain	102°–132° East, 18°–52° North

Some of the simulations have been carried out on a smaller sub-domain which is nested in the standard grid. The boundary conditions of the nested simulations are then provided by the simulation on the large domain. The resolution of the grid is not changed however. The smaller domain stretches from 112° to 122° East and from 35° to 45° North, Beijing is approximately at the center. This corresponds with the green domain plotted in figure 2.3. In the comparison plots (see figure 4.5, 4.7 and 4.2) the asterisk in the legend indicates which results are from simulations on the nested grid.

To study the effect on the concentrations of a simulation on the nested grid, a reference simulation is done which has the same settings as the standard simulation but using the smaller domain. The comparison plots compare the results of all simulations to the results of the reference simulation. It is noted that the reference simulation (which uses the nested grid) shows a reduction of the concentrations of PM10 compared to the standard simulation, most significant during the day. The maximum reduction is about eight percent, see figure 4.1.

When measurements are compared with model results (compare fig. 1.1A with fig. 1.1B) it can be seen that every pollutant suffers from high nocturnal concentrations, including PM10. PM10 is chemically not very active and a long-lived pollutant, its largest sink is precipitation (i.e. wet deposition, PM10 is not affected by dry deposition). Thus PM10 resembles a tracer. This means the

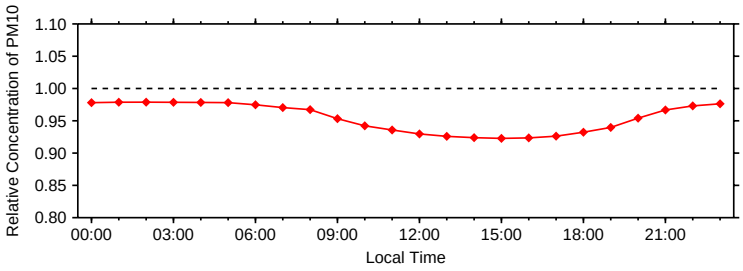

Figure 4.1: This plot compares the averaged concentration of PM10 from the reference simulation to the standard simulation.

problem is dynamically of origin rather than chemical. This is why all studies below are focused on PM10; it can act as a tracer for which the concentration is for the greatest part affected by dynamical processes. For the modelled PM10 surface concentrations to be comparable to the nocturnal measured concentrations it has to decrease by about 35%.

It has to be noted that *all results below are given as an average over a period from the 7th of August until the 30th of September in 2007* to be able to compare it to the measurements given in 1.1A.

Furthermore, the results of the lowest vertical layer have been interpolated to 116.40° longitude and 40.00° latitude using bilinear interpolation, which is the location of the Olympic park in Beijing. The measurements made by [Wang et al. (2008)] are representative for this location.

4.1 Sources and Sinks

4.1.1 Goal

To asses the ability of PM10 to be used as a tracer, the influence of its largest sink, precipitation, needs to be tested. Furthermore, since the sensibility of several dynamical parameters at Beijing are tested in section 4.3, it is needed to know how much influence they can possibly have and if the higher nocturnal concentrations can be caused by local errors in dynamical parameters. This depends on how much influence emissions in and near Beijing have on the concentration in Beijing. This needs to be explained.

Pollutants stemming from distant sources have dispersed and mixed on their way to Beijing. Thus this is a close to homogeneous (but not necessarily small) 'background' concentration. Thus local changes in dynamics, like a change in vertical mixing or a higher boundary layer height can not change this concentration significantly.

The change in PM10 concentrations of a surface layer grid cell, when neglecting chemistry, depends on the budget of advection and diffusion out of and the emissions into this cell and the magnitude of the sink. Local changes in vertical diffusion thus have a direct effect on its (change in) concentration. Furthermore, to be able to see this effect it may not be masked by its sinks.

When pollutants stem from near sources it may not be entirely homogeneous when reaching Beijing. This for example happens when a pollutant is emitted into a shallow boundary layer and then reaches a higher boundary layer in Beijing. Then this pollutant is dispersed, lowering its concentration. This means local changes in dynamics also affect the concentrations of pollutants stemming from near sources.

4.1.2 Simulation Setup

Three simulations have been carried out. The first shows the influence of its most important sink: precipitation. And the other two show the influence of the emission source on the concentration in Beijing.

Figure 4.2 shows the results of these simulations. Below the different simulations are summarized, see also table 4.1.

noprecip (NO PRECIPitation) The precipitation in the whole domain is set to zero.

Name	precipitation	emissions
noprecip	off	all
locemis	on	only Beijing
locemis2	on	10x10 around Beijing

Table 4.1: Summary of the simulations concerning sources and sinks.

locemis (LOCal EMISsions) Only the emissions stemming from the two grid cells containing Beijing are used, the emissions of the other grid cells are set to zero. See figure 4.3.

locemis2 (LOCal EMISsions 2) The emissions of a domain of 10 by 10 grid cells around (and including) Beijing are used. Now also the emissions of the closest big city Tianjin are taken into account. See figure 4.3.

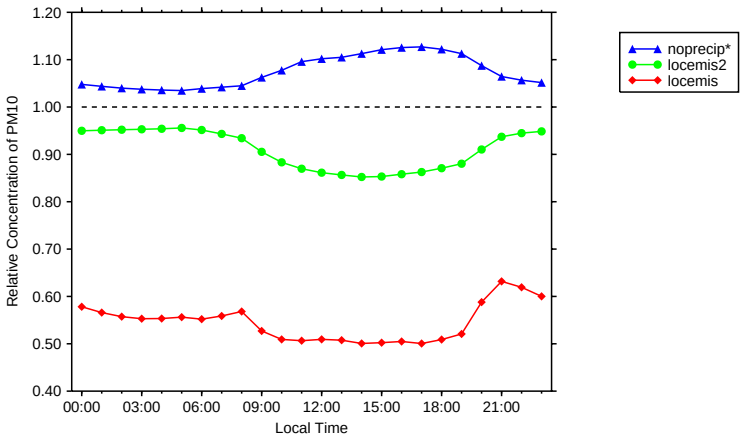

Figure 4.2: Results of simulations affecting the sources and sinks are compared with the results of the reference simulation for Beijing. The curves show the concentrations relative to the reference simulation. The asterisk in the legend indicates that the simulation was on the nested grid.

4.1.3 Analysis

Precipitation The influence of rain on the averaged PM10 concentration is about 5% during the night and about 13% during the day. Thus the larger part of PM10 is not influenced by precipitation and this sink is not expected to mask the dynamical effects on PM10, certainly not at night.

It is interesting to note that the effect of precipitation has a diurnal cycle and is most noticeable during the day. This is probably due to day time convection which help the forming of cumulus clouds which may start to rain out. Thus it rains more often during the day and this affects wet deposition.

Emission Sources From figure 4.4 it is seen that the prevailing wind direction is South. This means pollutants are advected from that direction. From figure 2.2 it can be seen that in the South and South West many pollutant sources

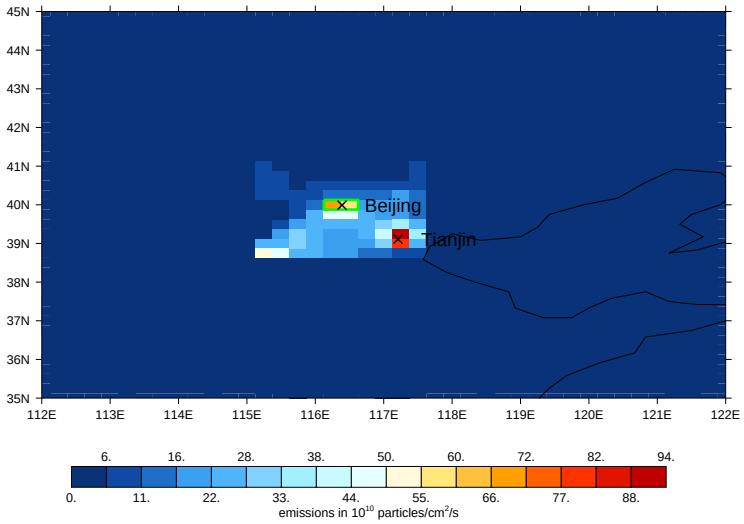

Figure 4.3: The emissions for PM10 as used in the 'locemis2' simulation. Surrounded by the green line are the two grid cells which emit during the 'locemis' simulation.

exist. This means the concentration of certain pollutants in Beijing is not only influenced by the emissions in Beijing itself, but also by emissions from the region outside (mainly South) of Beijing. Results from simulation 'locemis' and 'locemis2' confirm this. There it is seen that 50% to 60% stems directly from Beijing and 80% to 90% from the direct surroundings including Beijing. [Streets, (2008)] confirms this as well. This means local changes in dynamical parameters are suspected to have a possibly large influence on concentrations in Beijing.

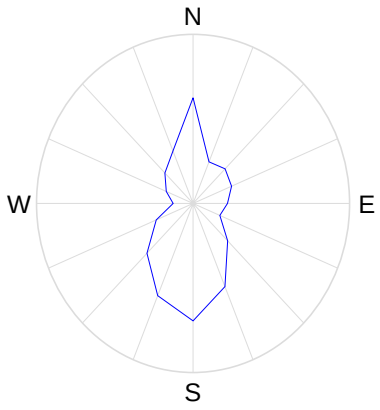

Figure 4.4: This plot shows a count of wind directions during September and August 2007 of the 10 m wind above Beijing as it was according to the ECMWF forecasts.

From figure 4.2 it can be seen that apparently during day time distant sources have a larger influence on PM10 concentrations than during night time. A possible explanation could be the next. Fore some reason the PM10 from a distant source is transported upward (e.g. by convergence) so its concentration closer to the ground is lower than higher above. Because the day time boundary

layer is higher than the nocturnal boundary layer, it can capture this higher PM10. Therefore day time concentrations are more influenced by distant sources compared to night time concentrations. This explanation is not checked and contradicts the assumption that distant sources are homogeneous. But the effect is small and it only enhances the argument that local changes in dynamics have a big influence on local concentrations.

This section shows that PM10 can be used as a tracer, i.e. its concentrations in Beijing are mainly influenced by emissions, advection and vertical diffusion. This makes it an ideal pollutant to visualize the influence of several parameters which influence these three features. It also shows that local changes in dynamical parameters can have a large influence on the pollutant concentrations in Beijing and thus the overestimated nocturnal concentrations can be caused by local effects.

4.2 Discretization

4.2.1 Goal

In principle the model output should be insensitive to the placement of the grid and, to a certain extent, to horizontal or vertical resolution and the time step chosen. When this is true there can be confidence that the model output is a consistent solution of the problem at hand.

Consistency means that the input data to the model and the model itself all contain the same phenomena and information. For example, Chimere should use the same topography as the model which calculates the meteorological data.

Consistency also means that the model is able to represent the important phenomena on the resolution of its grid and the time scale of the phenomena should not be smaller than the time step used by Chimere.

4.2.2 Simulation Setup

Four simulations have been conducted which test the models consistency. In figure 4.5 the results are shown. The plots show the concentration of PM10 relative to the reference simulation. Each name in the legend denotes a different simulation with a change in one or more parameters. Below the different simulations are summarized, see also table 4.2.

amfic1 For this simulation the size of the grid cells is enlarged. They are 0.5° in each direction instead of 0.25°. The meteo data is averaged.

hivres (HIgh Vertical RESolution) Instead of 8 vertical layers, this simulation uses 24 vertical layers.

shifted The grid is shifted half a grid cell (0.125°) in both directions. This means that Beijing now is entirely[3] in one grid cell. Beijing was originally split over two grid cells, this can be seen in figure 2.2 as a peak in the emissions.

[3]In Chimere Beijing is modelled by urban land use as surface (higher surface roughness and less biogenic emissions) and emissions. This means the urban land use is now entirely within one grid cell and there is a peak in emissions from that same grid cell.

Name	Grid size	Vert. Layers	$\Delta t^p / \Delta t^c$	shifted
amfic1	0.5°	8	10/10 min	no
hivres	0.25°	24	10/10 min	no
shifted	0.25°	8	10/10 min	yes
shortt	0.25°	8	5/2.5 min	no

Table 4.2: Summary of simulations concerning discretization effects.

shortt (SHORT Time step) The physical time step is reduced from 10 to 5 minutes and the chemical time step is reduced from 10 to 2.5 minutes. So there are two chemical time steps within one physical time step.

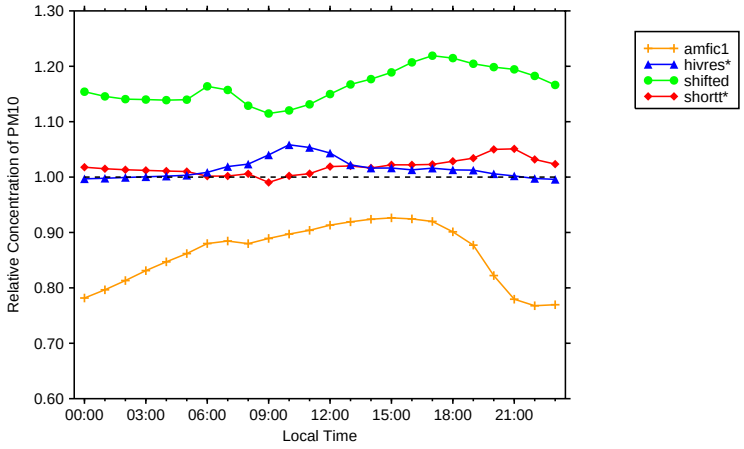

Figure 4.5: Results of several simulations affecting the discretization are compared with the results of the reference simulation above Beijing. The curves show the concentrations relative to that of the reference simulation. The asterisk in the legend indicates that the simulation used the nested grid.

4.2.3 Analysis

First it is noticed that 'hivres' and 'shortt' do not show much difference in PM10 concentrations. This means that the vertical resolution and time step are adequate for this simulation.

The 'shifted' simulation shows on average an increase of about 10% in PM10 concentrations. This is an unwanted situation since a change in the location of the grid should not change the simulation results.

The difference is due to limited spatial resolution. The PM10 emissions stem for a major part from traffic and are thus higher in urban areas compared to rural areas meaning Beijing is in general more polluted than its surroundings. The concentration in a grid cell should be interpreted as the averaged concentration in the area where it is located. In the grid cell (partially) containing Beijing the concentration is an average between Beijing and its surroundings, and thus lower than the concentration in Beijing. If Beijing is entirely within one grid cell, the average of this grid cell is less influenced by the surroundings and thus a better representative for Beijing and thereby higher in value.

In the model this is reflected by the fact that Beijing is divided over two grid cells in the original grid, and in the shifted grid Beijing lies entirely within one grid cell. This means that for the shifted grid all the emissions from Beijing are concentrated in one grid cell so the spatial peak in emissions is much higher compared to that in the original grid. Since the advection and the diffusion terms do not change significantly, this leads to a higher concentration.

Simulation 'amfic1' shows a reduction of 15% to 25% in PM10 concentrations. This can be explained by the same argument as for 'shifted'. The grid cells in amfic are larger and thus less representable for Beijing (it has only 11% urban land use). This means the emissions are lower in this grid cell. Also, because of the lower resolution, both the discretization error as the numerical diffusion increases. Whether a larger discretization error results in a lower or higher concentration is not immediately clear but the numerical diffusion causes the PM10 to disperse horizontally more rapidly causing lower concentrations. This simulation also shows a diurnal cycle but no explanation has been found for this.

Simulations 'amfic1' and 'shifted' suggest that the model should always underpredict the concentrations in Beijing because a grid cell of the size used in the standard simulation will always contain rural land. Linear interpolation to Beijing cannot undo this effect and reproduce the higher concentrations in Beijing.

Last it should be noted that the land use data is outdated. It stems from a survey in the period 1981-1994. In this data the two grid cells containing Beijing have an urban coverage of about 16% to 20%. Since that time Beijing has grown rapidly. Right now Beijing would roughly cover the area of about three grid cells. However, in Chimere this influences only the dry deposition, biogenic emissions and surface roughness. For PM10 only surface roughness can influence its concentration indirectly through a higher vertical diffusion coefficient. To what extent will be covered in the next section. The emission database is from 2006 which is reasonably up-to-date.

It is shown that the model shows some inconsistency. The emission data does not correspond with the land use data. Furthermore, the limited spatial resolution should rather underestimate than overestimate the concentrations in Beijing. This means that the fact that Chimere results overpredict the nocturnal PM10 concentrations is not explained by discretization.

4.3 Boundary Layer Parameters

4.3.1 Goal

Measurements of the boundary layer height above a large city are rare, especially at night. Data from Athens [Tombrou et al. (2007)] suggest a nocturnal boundary layer height of around $500\,m$ during fair weather conditions in September. Fair weather conditions (clear sky and low wind speeds) produce the lowest nocturnal boundary layers. Athens is on about the same latitude as Beijing, however, in contrast to Beijing, Athens is close to the sea which makes them not easily comparable. Model results from Beijing made with a model including the effects of a city on the boundary layer height (presented in chapter 5 of this report) suggest a nocturnal boundary layer height of around $200\,m$ during fair weather conditions. This shows a minimum value of $20\,m$ is much too low. The

ECMWF data shows that on many occasions the modelled nocturnal boundary layer above Beijing is reduced to this minimum value. This does not seem realistic.

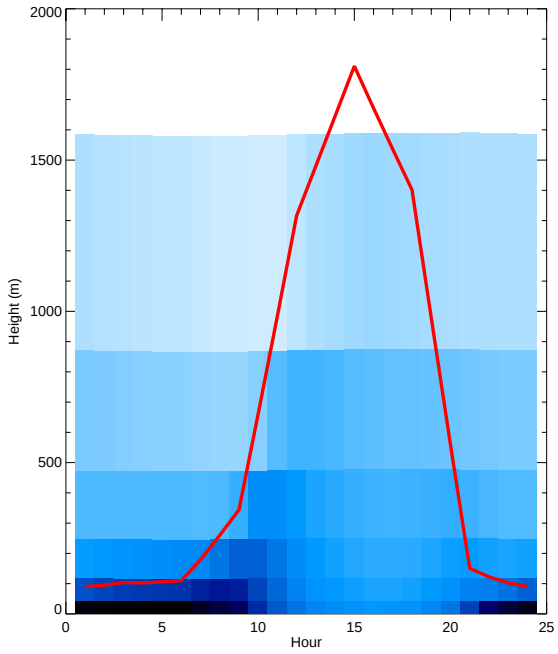

Figure 4.6: The PM10 concentrations of the vertical column above Beijing of the reference simulation is shown in blue tints. The darker the shade, the higher the concentration. The red curve is the boundary layer height. Both the concentrations and the boundary layer height are averaged over August and September 2007.

The nocturnal boundary layer has two important parameters: the vertical diffusion coefficient (K_z) and the boundary layer height. These parameters have a large effect on the concentrations in Beijing. This is because the space in which a certain amount of pollutant can be emitted during a time step is bounded by the horizontal advection and the atmospheric boundary layer height. But since the pollutants are being emitted at ground level, the vertical diffusion coefficient dictates how much of this vertical space is being used, see figure 4.6. This means that both an increased boundary layer height and a higher diffusion coefficient results in a larger space in which the emitted pollutant can spread resulting in lower concentrations.

Furthermore, the surface roughness has an effect on the vertical diffusion coefficient (not on the boundary layer height, see section 3.6). The results of the simulations discussed in this section will give insight in how these three parameters influence the PM10 concentrations in Beijing.

4.3.2 Simulation Setup

Figure 4.7 shows the results of four simulations. Below the difference in setup of the different simulations is summarized, see also table 4.3

hikz (HIgh KZ) In this simulation the minimum value for the vertical diffusion

Name	min(K_z)	min(BLH)	urban land use
hihhikz	$1.0\,m^2/s$	$750\,m$	15.6%/19.9%
hikz	$1.0\,m^2/s$	$20\,m$	15.6%/19.9%
urblu	$0.1\,m^2/s$	$750\,m$	100%/100%
hih	$0.1\,m^2/s$	$750\,m$	15.6%/19.9%

Table 4.3: Summary of simulations concerning boundary layer parameters.

coefficient is set to $1.0\,m^2/s$ instead of the reference value of $0.1\,m^2/s$.

hihhikz (HIgh blH HIgh KZ) Same as 'hikz' but now also the boundary layer height is increased to a minimum of $750\,m$.

urblu (URBan Land Use) Here the land use of the two grid cells containing Beijing are set to 100% urban land use. This has an effect on the surface roughness. The surface roughness has an effect on the vertical diffusion coefficient. The boundary layer height is set to a minimum of $750\,m$.

hih (HIgh blH) The minimum boundary layer height is set at $750\,m$ for the two grid cells containing Beijing in this simulation.

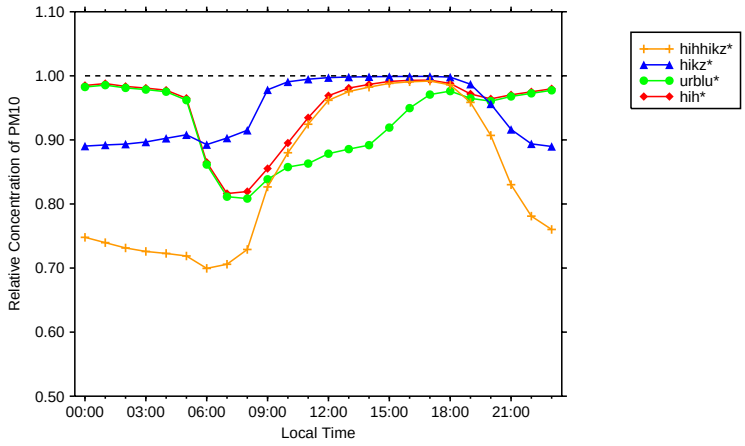

Figure 4.7: Seven simulations concerning boundary layer parameters are compared with the standard simulation above Beijing. The curves show the concentrations relative to the standard simulation. All these simulations use the nested grid.

4.3.3 Analysis

Surface Roughness It has been noted earlier that the land use database is outdated. This database has in general an effect on the biogenic sources, the dry deposition of the trace gasses and on the surface roughness. PM10 concentrations are only altered because of the change in surface roughness which changes the value of K_z.

To see the effect of this change a simulation has been performed for which the result is plotted in figure 4.7 as 'urblu'. The urban land use of the two

grid cells containing Beijing is set to 100% for this simulation. The original values were 15.6% and 19.9%. The minimum boundary layer height is set to $750\,m$. This is because the maximal effect is sought meaning no influence of the boundary layer height is wanted.

To see the impact of this change in land use, results of simulation 'urblu' should be compared with those of simulation 'hih' because its minimum boundary layer is also set to $750\,m$. The change in land use has only an effect during the day of at most about 10%. This change is due to a change in K_z because the boundary layer height is not influenced by the difference in roughness.

The reason that almost no change is observed at night is because in this period the K_z values are set to the minimum value of $0.1\,m^2/s$ almost every night in the reference simulation (52 out of 55). In the 'urlu' simulation this is still the case (again 52 out of 55).

The above discussion leads to the conclusion that the out dated land use data can not explain the higher modelled nocturnal PM10 concentrations compared to measurements.

Boundary Layer Height and Vertical Diffusion In run 'hih' the boundary layer height of the two grid cells containing Beijing is set to a minimum height of $750\,m$ instead of $20\,m$ in the reference run. A minimum height of $750\,m$ is exaggerated but this simulation is meant to show the qualitative effect.

For this simulation the PM10 concentrations do not deviate far from the results of the reference simulation except around sunrise and, to lesser extent, sunset (see figure 4.7). This shows that the vertical diffusion coefficient actually is the limiting factor to the vertical dispersion. Except during sunrise and sunset, there the boundary layer height apparently is the limiting factor.

In the reference simulation the minimum value for the vertical diffusion coefficient (K_z) is reached almost every night (51 out of 55) over the whole depth of the boundary layer during August and September 2007. For simulation 'hikz' the minimum value of K_z is set to $1.0\,m^2/s$ instead of $0.1\,m^2/s$. Typical values for the day time (mixing layer) coefficient are around $10\,m^2/s$ to $15\,m^2/s$. No examples of nocturnal values of K_z have been found so determining the minimum value is a bit arbitrary, however, [Foy et al. (2007)] use the same minimum for some of their simulations. Furthermore the qualitative effect is again pursued.

Results of simulation 'hikz' show that during the night the increase of the minimum value of K_z leads to a reduction of nocturnal PM10 concentrations of about 10%, daily values are not altered. This is the result wanted, however, 10% reduction is low compared to the sought 35%. Figure 4.6 shows that the vertical mixing is also limited by the boundary layer height. On average this height is in the second vertical model layer which means PM10 can only spread over these two cells.

To study to what extent the boundary layer height is the limiting factor for PM10 concentrations when K_z is increased, simulation 'hihhikz' has been carried out. This changes both the minimum value of K_z from $0.1\,m^2/s$ to $1.0\,m^2/s$ and the minimum value of the boundary layer height from $20\,m$ to $750\,m$. This simulation shows a nocturnal reduction of PM10 concentrations of about 25% to 30%. This close to the sought value of 35%. This means that for an effective reduction of the nocturnal PM10 concentrations both K_z and the

boundary layer height must be increased.

At night during fair weather conditions the boundary layer above rural areas usually becomes stable, however, it has been observed (e.g. [Oke, (1995)], [Mestayer and Anquetin, (1995)]) that the boundary layer above a city usually fails to become stable in such conditions. It is neutral or even becomes unstable. Chimere uses the Obukhov length (see equation 3.23) as switch between the K_z formulation for stable and unstable cases (see section 3.6). Since the Obukhov length is not dependent on the boundary layer height but on sensible heat flux, there is no change in the choice of which formulation is used. However, in reality the higher boundary layer height would be due to a higher sensible heat flux. This means that in run 'hih' the wrong formulation for K_z is used when the ECMWF boundary layer is recognized as stable.

The above discussion leads to the conclusion that for a significant decrease in nocturnal concentrations, both the nocturnal boundary layer height and the vertical diffusion coefficient must be increased. The vertical diffusion coefficient is strongly dependent on the sensible heat flux, this means that for a realistic formulation also the nocturnal sensible heat flux must be increased. The reason for a higher sensible heat flux is the presence of a heat island effect. In an urban area, like Beijing, heat is trapped which causes a higher sensible heat flux and thus a higher boundary layer height, see [Souch and Grimmond, (2006)] and chapter 5. This effect is strongest during the night meaning it could potentially explain the high nocturnal PM10 concentrations.

The influence of the heat island on nocturnal trace gas concentrations is confirmed by [Sarrat et al., (2006)]. They compare model simulations of NO_x and O_3 with measurements above Paris. Paris is very comparable to Beijing in a meteorological sense. Both cities have a relatively smooth topography and are located inland far from the sea. Beijing does however have mountain ranges at its North and West side which start at around $25\,km$ distance.

[Sarrat et al., (2006)] have done two simulations, one with the urban heat island incorporated and one without. They also simulate large peaks (about a factor two higher compared to measurements) in NO_x during the night which are not measured and not simulated when the heat island effect is incorporated. The boundary layer heights they calculated are $206\,m$ and $72\,m$ during the night for urban and non urban conditions respectively. This shows a large influence of the heat island.

[Sarrat et al., (2006)] also show an increase in the boundary layer height during day times. However, [Tombrou et al., (2007)] show by comparing different boundary layer parameterizations with observations that nocturnal boundary layer heights can be quite well captured by an urban parameterization but daily urban boundary layer heights are overestimated by the model they use. The parameterizations of the urban boundary layer used by Sarrat and Tombrou are not the same, but it does show the uncertainty involved.

4.4 Hong Kong

Unfortunately no measured hourly concentrations of PM10 (or other species) are available for Beijing. Because of this, and in order to have an other example of the overestimated nocturnal PM10 concentrations, Hong Kong data is analyzed.

In Hong Kong, as opposed to Beijing, also the hourly concentrations of the whole period of August and September in 2007 are available. The environmental

protection department in Hong Kong has a web site (`http://epic.epd.gov.hk/ca/uid/airdata/p/1`) from which hourly concentrations from different locations in and around Hong Kong are downloadable. The data goes back to 1990. There are two kinds of air quality measurement stations: three roadside and eleven general stations. To avoid too strong signals from traffic, only the general stations are used, the measurements from these eleven stations are averaged. The simulated data from Chimere is interpolated to the average location of the stations (22.4° North and 114.2° East).

The result is shown in figure 4.8. Here the measured concentrations of PM10 are compared to the result of the standard simulation (no nested grid is used here, the reference simulation has been carried out on the nested grid). Here the same trend as in Beijing is seen. During the day the predictions are close to those of the standard simulation but during the night model results show higher concentrations than measured data.

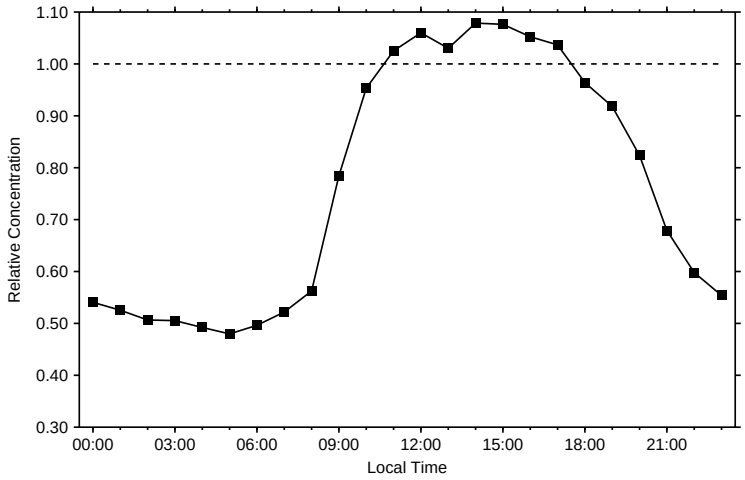

Figure 4.8: Relative PM10 concentrations of the measured data compared to the results of the standard simulation in Hong Kong

Hong Kong is located in a river delta near mountains and at the coast. This means that the terrain is highly inhomogeneous and there is an influence from the sea. This gives a different behavior of the boundary layer. As can be seen from figure 4.6 the boundary layer at night is much higher but during the day much lower.

4.4.1 Analysis

Hong Kong has a much higher nocturnal boundary layer compared to Beijing as can be seen from comparing figure 4.6 with figure 4.9. During most nights (48 out of 55) the boundary layer is unstable and thus the unstable formulation for K_z is used. However the pollutants still pile up in the bottom layer (see figure 4.9). Thus for more realistic PM10 concentrations the nocturnal values of K_z should be increased, this means the sensible heat flux must be increased (see section 3.6).

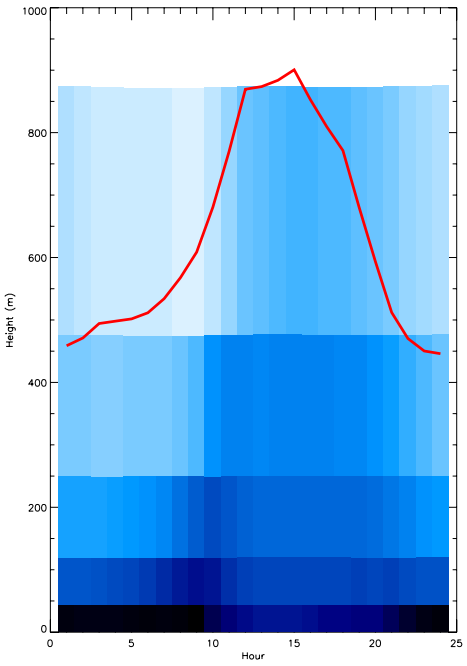

Figure 4.9: The PM10 concentrations of the vertical column above Hong Kong in the standard simulation is shown in blue tints. The darker the shade, the higher the concentration. The red curve is the boundary layer height.

4.4.2 Comparisons with Measurements

Several scatterplots are produced from the available data. Figure 4.10 C shows that Chimere performs well on average, however, a large spread is observed. Note that a large part of the outlying data lies above the black line which means that Chimere overpredicts the pollutant concentrations.

In figure 4.10 A and B a distinction is made between daytime values and night time values. It shows an underprediction during the day and an overprediction during the night.

From figure 4.11 more insight can be obtained. During daytime Chimere indeed appears to underpredict the measurements but the trend including extremes are predicted quite well. During the night Chimere clearly over predicts the measured data. But it also predicts extremes (spikes) at times when none are measured, i.e. at 19th and 26th of August, 6th of September and 16 to 23 September. These two months are very wet for Hong Kong and these nights coincide with dry periods. When the rain stops, nocturnal concentrations immediately deviate from measurements.

It is shown that Chimere systematically under predicts the daily values of PM10. The cause is not studied but it can be due to the fact that grid cells covering Hong Kong also contain rural land which lowers the average concentration in a grid cell, the 11 measurement stations are mainly located at urban sites. The effect of the heat island on the boundary layer height is small during the day.

An other explanation for the lower daily concentrations can be the fact that

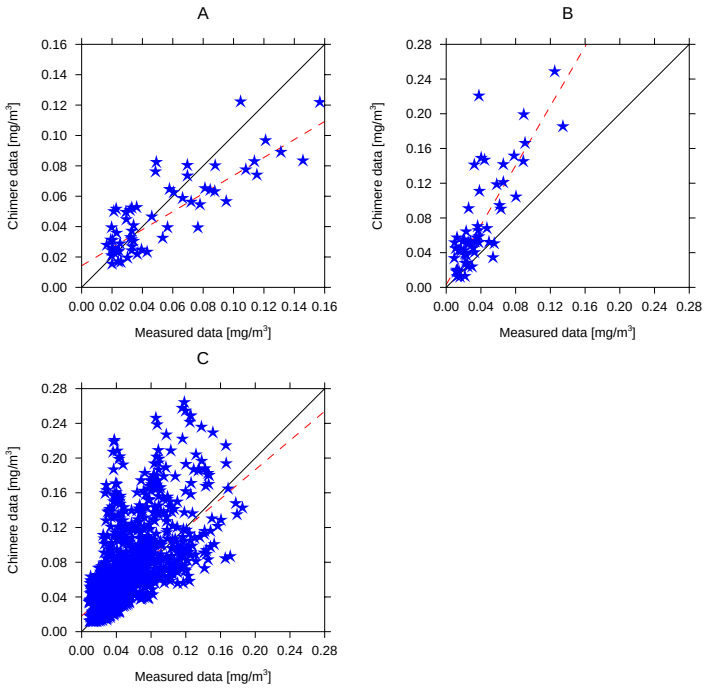

Figure 4.10: Measured against modelled data at (A) 3PM, (B) 3AM and (C) every hour for the months August and September 2007 from Hong Kong. The red dashed line is calculated using the 'least absolute deviation' method. This gives less weight to outlying data compared to a least squares method.

ECMWF models over predict vertical mixing of momentum leading to a higher mixing layer (i.e. daily boundary layer) [Cuxart et al. (2006)]. The reason for this are the better forecast skill scores obtained by overpredicting vertical mixing (or actually, by implementing different so called surface similarity functions leading to higher vertical mixing) [Beljaars, (1995)]. However, this leads to higher sensible heat fluxes which lead to a higher vertical diffusion coefficient which on its turn leads to a reduction in PM10 concentrations.

A third explanation could be that the emission data is from one year earlier. The fast growth of the Chinese economy could in this case (partially) explain the lower daily modelled concentrations.

4.5 Conclusions

Because the influence of precipitation does not mask the dynamical effects on the concentration of PM10, it can act as a tracer in Beijing. This means it can be used to study the dynamics of Chimere as has been done in this chapter. The influence of precipitation does have a larger impact at the day compared to the night, this is probably because there is more precipitation during the day.

It is also shown that the local changes in dynamics can influence at least 50% but probably a larger part of the amount of PM10 in Beijing. 35% reduction is

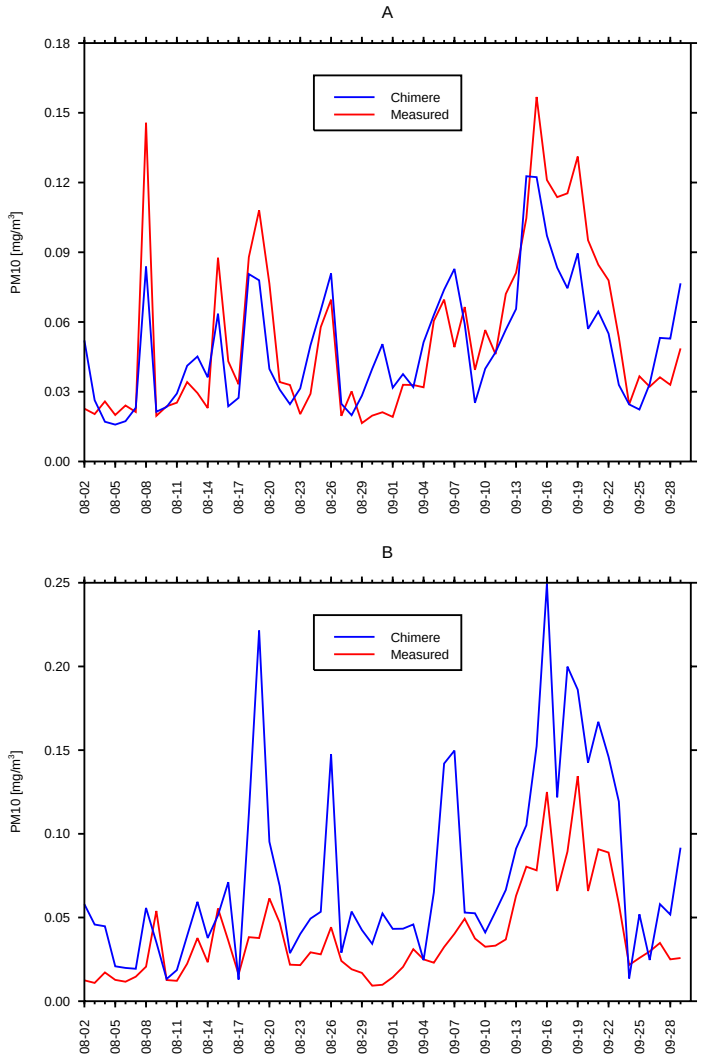

Figure 4.11: For every day in the period of August and September 2007 the PM10 concentration at (A) 3PM and (B) 3AM from measurements and Chimere calculations from Hong Kong are compared. Chimere greatly overestimates nocturnal values at 19 and 26 Augustus, 7 September and the period from 16 to 23 September. These periods correspond to periods without precipitation.

needed for modelled nocturnal concentrations to compare with measured concentrations. This is enough to correct for the higher nocturnal concentrations and thus the higher nocturnal concentrations are possibly due to local effects. The PM10 concentration in Beijing is more affected by distant emission sources during day times compared to night times. This might be due to the movement of pollutants upwards which are captured by day time boundary layers.

The vertical resolution and the time step are adequate to model the air

quality above Beijing, however, when the grid is shifted the PM10 concentration increases with maximal 15%. This can be explained by the fact that Beijing is entirely within one grid cell in that case. This means the emissions are more localized and thus higher in that grid cell. Decreasing the horizontal resolution decreases the PM10 concentrations. This is caused by the same but opposite effect as when the grid is shifted. The emissions from the grid cell containing Beijing are averaged over Beijing and its surroundings resulting in a lower value. It can be concluded that discretization does have an effect on the PM10 concentrations in Beijing but it can not explain the higher nocturnal values of PM10.

The boundary layer above Beijing can become as low as $20\,m$ according to the ECMWF model. This is unrealistically low. But when the boundary layer height is increased, no significant change is observed. This is due to low K_z values; the PM10 is trapped at the surface. Surface roughness can not significantly increase K_z, so an increase in sensible heat flux is needed. This increase can only be physically justified by the presence of an urban heat island. The ECMWF does not incorporate this effect. During day times its influence is small but during night times it can lead to significant errors.

5 Boundary Layers of Cities

In the preceding chapter it was concluded that the effects a city has on nocturnal pollutant concentrations is not properly modelled by Chimere because it is not included in the ECMWF data that it has as input. In this chapter the effects of a city on its surroundings, called the heat island effect, and the proper way to implement this is discussed. Also a case study with a model including the heat island effect has been carried out and in the last section simulations have been performed using the knowledge of the urban heat island effect.

5.1 The Urban Heat Island

The urban heat island is simply the characteristic temperature of either the surface or the air in a city which is higher than its surroundings. It is found in cities of almost all sizes. It carries its name because of the isotherms of the temperature field of a city look like the topographic contours of an island.

At present urban climate is given much research attention. Because of its complexity not all aspects are thoroughly understood. There are many parameters influencing urban climate e.g. building height, building density, surface inhomogeneity, the prosperity of its inhabitants and even roof design. Using only the most important parameters gives promising results in modelling the urban heat island. Three important parameters can be identified, from [Mestayer and Anquetin, (1995)]:

Latent Heat In rural areas precipitation is absorbed by the ground and later by vegetation. The vegetation evaporates it to take in nutrients from the soil. Since urban areas have little vegetation and most cities have an efficient sewer system to drain precipitation, much less moisture is evaporated there. This means that the excess energy normally used in the evaporation process now contributes to the sensible heat flux and the heat storage. This means that the Bowen ratio (ratio between sensible and latent heat flux) increases. For rural areas typical ratios are in the order of 0.4, for suburban areas 1.2 and for urban areas 3 [Piringer et al., (2007)]. Because of the large latent heat of evaporation of water, this is one of the major causes of the heat island.

Heat Storage Vegetation uses incoming solar radiation as a source of energy. Since in urban areas there is less vegetation this energy cannot be converted and thus is stored in e.g. buildings or roads. This energy is released after sunset. The heat storage varies between 15% to 30% of the total heat budget. The heat storage accumulates during the day and is progressively released to the air during the night. Heat storage is often the largest sink of heat during the day and always the largest source at night, when it almost balances the radiative heat loss. This explains the large values of the heat island in terms of air temperature during the night.

Anthropogenic Heat The use of fossil fuels contributes significantly to the total energy budget. The strength of anthropogenic heat strongly depends on the city itself. For example, data from Vancouver as treated in [Oke, (1995)] suggest a anthropogenic flux of about 11 and 7 W/m^2 for day and

night, respectively. And according to [Crutzen, (2004)] typical anthropogenic heat flux values for urban areas are 20-70 W/m^2. [Oke, (1995)] notes that in most cities the anthropogenic heat flux alone is unlikely to be a major contributor to the urban heat island. However, Beijing is a megacity and its anthropogenic heat flux during rush hour, at 08:00hr local time, in summer has been measured to be more than 200 W/m^2 [Chen et al. (2009)]. For comparison, on average the energy of the sun as absorbed by the surface in Beijing is typically around 500 W/m^2 at noon when no clouds are present. Thus the anthropogenic heat in Beijing is of the same order of magnitude as compared to the solar energy.

Figure 5.1 shows a typical diurnal evolution of the heat island effect in terms of heat and temperature. The most notable features are:

- The much higher sensible heat flux compared to latent heat flux.
- The sensible heat flux failing to turn negative during the night.
- The considerable heat storage during the day and release during the night.
- The considerable anthropogenic heat flux.

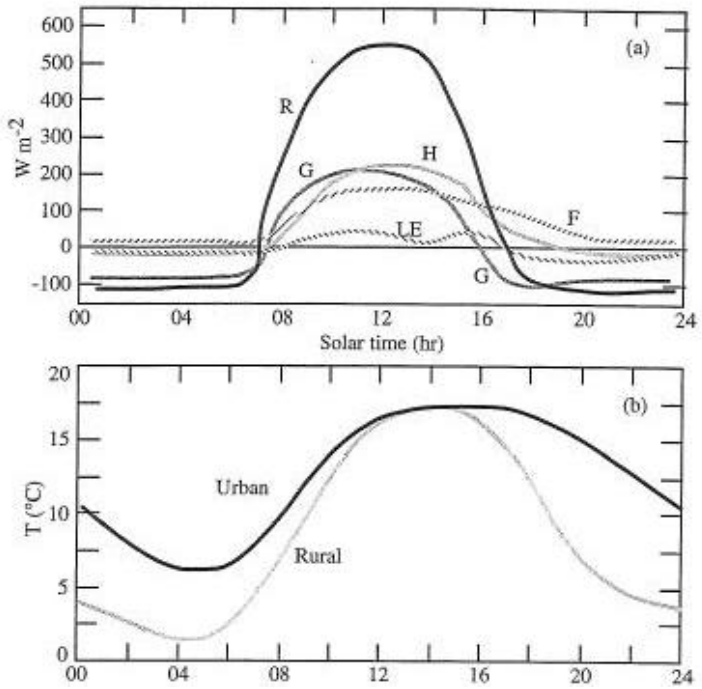

Figure 5.1: Typical, schematic diurnal evolution of (a) the heat budget terms over the urban canopy. R is radiation budget, G is heat storage, H is sensible heat, F is anthropogenic heat and LE is latent heat. Figure (b) is a typical diurnal evolution of urban and rural air temperatures. Solar time is time is the time as synchronized with the sun, so at 12hr the sun is in zenith. Copied from [Mestayer and Anquetin, (1995)].

Due to the release of stored heat at night, which results in an increase in sensible heat flux, and the anthropogenic heat, the boundary layer above a city usually fails to become stable at night. It is observed to be neutral or even unstable (e.g. [Piringer et al., (2007)]). This enhances the vertical mixing and increases the nocturnal boundary layer height.

Other effects also play a role. The effective albedo (surface reflectance) of a city is lower, meaning more energy is absorbed. This has two reasons. It is because materials, like concrete or tarmac, have a lower albedo compared to natural surfaces and because incoming radiation undergo multiple reflections on building walls and the surface in between. An other effect is the limited sky view factor in a city. A large area of flat land can radiate to 180° of sky. But because of surrounding buildings most roads and building walls can only radiate to a fraction of this. This means that during the night heat is trapped because it is not able to radiate away freely. However, these effects are limited. The total radiative budget above an urban area is comparable to the rural total radiative budget [Mestayer and Anquetin, (1995)]. Thus the radiative budget is not the main cause of the heat island.

Wind also has a strong influence on the heat island. According to [Oke, (1995)]: "*Auer and Changnon (1977) found the [Urban heat island], the vertical extent of its thermal anomalies, and the amount of "doming" of the [urban boundary layer] to be inverse linear functions of the wind speed in the mixing layer. Hildebrand and Ackerman (1984) also note the [Urban heat island] to be inversely related to wind, and further that urban anomalies of [the sensible heat flux], vertical turbulent kinetic energy and total turbulent kinetic energy all decreased as wind speed increased.*". The "doming" that Oke refers to is the dome like circulation that forms when winds are low as plotted in figure 5.2b. In the period from August and September 2007 in Beijing there were 54 out of 55 nights with a 10m wind less than $2.5\,m/s$. This means a large influence of the urban heat island can be expected.

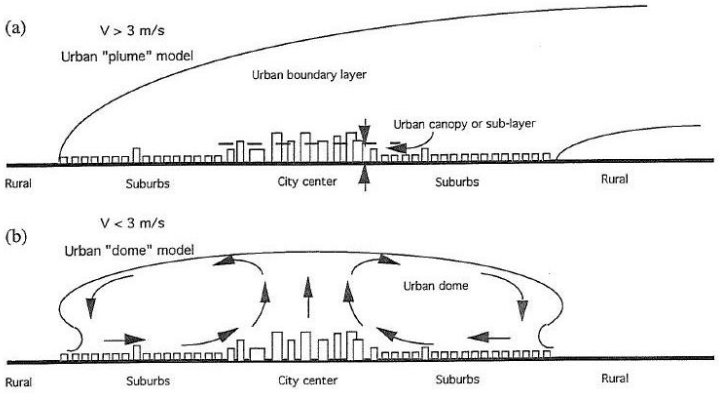

Figure 5.2: Models of the urban heat island in conditions of (a) moderate to strong wind and (b) weak wind. Copied from [Mestayer and Anquetin, (1995)].

[Tombrou et al., (2007)] have carried out a model evaluation for the atmospheric boundary layer height above an urban area. They conclude that for the urban scheme, the incorporation of both anthropogenic and storage heat release provides promising results for urban applications. Their results suggest these

two factors are most important when modelling the boundary layer height. The change in Bowen ratio is also incorporated in their simulations.

5.2 Case Study

To see the effects of Beijing on the boundary layer height a case study has been carried out with two models both incorporating the effects of a heat island. Both simulations have been carried out by Gert-Jan Steeneveld who is a researcher at the Meteorology and Air Quality Group within the Meteorology and Physical Climatology Section from Wageningen University.

The coupled WRF/Unified Noah/Urban-Canopy modeling system consists of three coupled models. The first is the 'Weather Research and Forecasting' (WRF) model. This is a 3-D meso-scale numerical weather prediction system (`http://www.wrf-model.org`). The Unified Noah model is a land surface model, it couples the land surface to the atmosphere, it is described in [Ek et al., (2003)]. And the Urban-Canopy model is described in [Kuska and Kumura, (2004)]. The urban canopy is the layer between the surface and the average roof top of a city. This model describes all effects mentioned in section 5.1.

The simulations with the WRF model have been nested in the NCEP (National Centers for Environmental Prediction, `http://www.ncep.noaa.gov/`) global weather forecasting model. The simulations with the WRF model have been carried out for two domains. The first and largest domain uses 60x60 grid cells with a resolution of $12\,km$ with Beijing or Hong Kong in its center. The second and smaller domain is nested in the first and uses 100x100 grid cells with a resolution of $4\,km$. Two days have been simulated, one in Beijing from 24-09-2007 1800UTC until 28-09-2007 03UTC, and one for Hong Kong from 25-08-2007 00UTC until 27-08-2007 06UTC. These periods have been chosen for their fair weather conditions (i.e. low winds and no clouds).

The 1-D (single column) model described in [Steeneveld et al., (2006)] has been developed to be able to model especially stable boundary layers with a high vertical resolution both in the atmosphere as in the ground. This model is used for simulations both for the rural and for the urban situation for two periods: 25-09-2007 03UTC until 26-09-2007 03UTC for Beijing and 26-08-2007 03UTC until 27-08-2007 03UTC for Hong Kong. These periods overlap with the simulations carried out with the WRF model. It uses forcings from the ECMWF model, an extra anthropogenic heat flux of $25\,W/m^2$, a higher surface roughness ($1\,m$ instead of $0.3\,m$ for the rural simulation) and a high canopy resistance of $1400\,s/m$ compared to $100\,s/m$ for the rural simulation. The canopy resistance is a resistance to the latent heat flux next to the aerodynamic resistance. It is used to model the amount of water evaporated by plants and trees, this also depends on ground moisture. The value for the canopy resistance of $100\,s/m$ is a reasonable first order estimation for a rural site (in reality it is dependent on meteorological conditions like humidity and temperature). The rural value of $1400\,s/m$ is an educated guess. So as far as the the heat island effect is concerned, this model only simulates the anthropogenic heat flux, the extra roughness and the decrease in latent heat flux.

The results are shown in figure 5.3 and 5.4. During day time ECMWF predicts the highest boundary layers. In section 4.5 it is noted that ECMWF predicts too high mixing layers to produce better forecasts, this could be an explanation. In Hong Kong the difference between WRF and ECMWF is quite

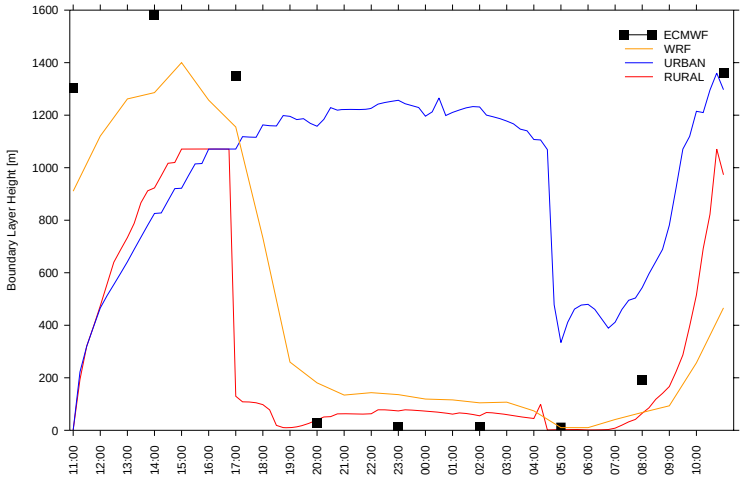

Figure 5.3: Boundary layer heights of the WRF model, the single column model for both rural and urban situations and the ECMWF model starting at 25-09-2007 11hr local time above Beijing. Courtesy Gert-Jan Steeneveld

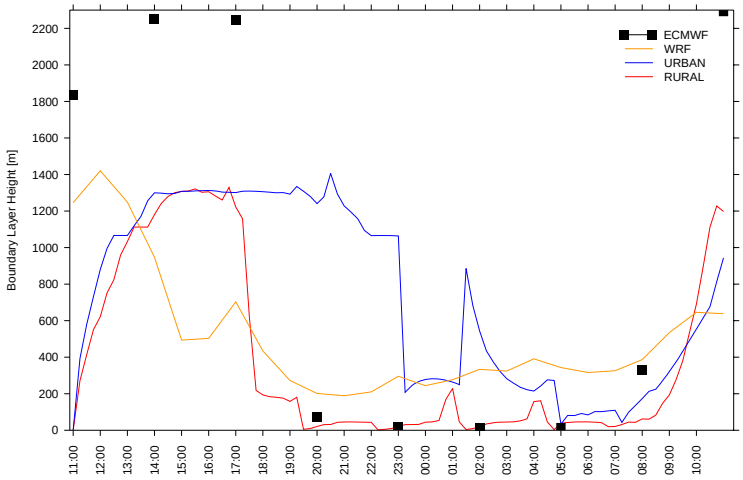

Figure 5.4: Boundary layer heights of the WRF model, the single column model for both rural and urban situations and the ECMWF model starting at 26-08-2007 11hr local time above Hong Kong. Courtesy of Gert-Jan Steeneveld

dramatic. However, Hong Kong has a very inhomogeneous topography and is close to sea. This means that on a higher model resolution these influences are better resolved and may have an effect on the boundary layer.

During the night WRF and the 1D-Urban simulations differ dramatically. This highlights the uncertainty there still is in modelling the urban boundary layer. The difference may be due to the mesoscale changes in wind and temperature fields which are resolved by the WRF model because of its higher spatial resolution but are not introduced in the single column scheme. [Chen et al., (2009)] show simulations of the low level jet (a feature at the top of the nocturnal boundary layer) above Beijing at an altitude of about $200\,m$, also

during fair weather conditions. This points in the direction of the WRF simulation to be more correct. Other studies (e.g. [Oke, (1995)], [Sarrat (2006)] [Tombrou, (2007)] [Pino et al., (2004)], [Lemonsu and Masson, (2002)]) also show a nocturnal urban boundary layer in the order of a few hundred meters and not kilometers. Furthermore they show that the nocturnal boundary layer is usually smaller than mixing layers. Thus the WRF simulations appear more correct on the nocturnal urban boundary layer height.

The prediction of the nocturnal urban boundary layer in WRF also depends on correct and high resolution input data for land use, surface albedos, anthropogenic heat flux, heat capacities and more parameters. Since this data is not available to us for Beijing or Hong Kong, uncertainty remains about the actual boundary layer height. And even with correct input data, the model itself may still contain uncertainties in its assumptions. In [Grimmond et al., (2009)] 25 different parameterization schemes are compared. It shows that a more complex parameterization scheme does not necessarily perform better. It is demonstrated that the schemes do perform better than schemes which do not take the heat island effect into account (e.g. [Tombrou et al., (2007)] or [Piringer et al., (2007)]).

The 1D-Urban simulation shows for Hong Kong a sudden dip at 23:00hr followed by a sudden rise at 01:15hr. The dip coincides with a sudden fall in geostrophic wind speed and the rise with a sudden large change in direction of the geostrophic wind. The model is very sensitive to these parameters. This event, however, appears not correctly modelled.

The single column simulation for the rural case is during the night quite well in agreement with the ECMWF data. This shows that ECMWF indeed predicts rural boundary layer heights and no significant urban effects are taken into account.

The case studies show that the nocturnal boundary layer from ECMWF does not contain any significant urban heat island effects. They also suggest that the nocturnal urban boundary layer is around $150\,m$ to $200\,m$ in fair weather conditions. This is in general agreement with studies in other cities.

5.3 Implementation of the Heat Island Effect in Chimere

Two final simulations are carried out which use all the acquired knowledge. The first uses the options already available in Chimere, the second changes more variables. The result is plotted in figure 5.5.

Chimere has some possibilities to correct for the heat island effect when it is not in the meteorological input data. It can set a minimum value for the boundary layer height, add an anthropogenic heat flux and scale the surface wind. These parameters are scaled by the percentage of urban land use in a grid cell. For Beijing these percentages are 16% and 20%.

The option to scale the surface wind is not used because its value should strongly depend on wind speed and time of day. During the day no change in concentrations is wanted, so no correction should be made. Furthermore, when wind speeds are low, 'dome' forming can occur (see fig. 5.2a) which can increase the wind speeds [Oke, (1995)]. However, the roughness usually lowers the wind speeds when these are moderate to high. [Rigby and Roumi, (2008)] propose a very simple method to include the heat island effect of London in the ECMWF data for their dispersion models. They increase the wind speed

when it drops below $3\,m/s$ and lower it otherwise. In this way they are able to get better statistics on pollution modelling. It shows the surface wind speed does not necessarily have to be reduced to obtain better results as might be expected. Thus setting a constant value to scale the wind does not seem to help. The settings of the two simulation are summarized below.

ChimOpts An anthropogenic heat flux of $200\,W/m^2$ is added and the minimum boundary layer height is set to $200\,m$, these parameters are scaled by urban land use percentages (15.6% and 19.9%).

h200anth An anthropogenic heat flux of $200\,W/m^2$ is added which is scaled by the urban land use percentages. A minimum boundary layer height is set to $200\,m$ for the two grid cells containing Beijing, this is not scaled by urban land use percentages. A minimum value for K_z is set to $1.0\,m^2/s$ and the formulation for unstable K_z is always used.

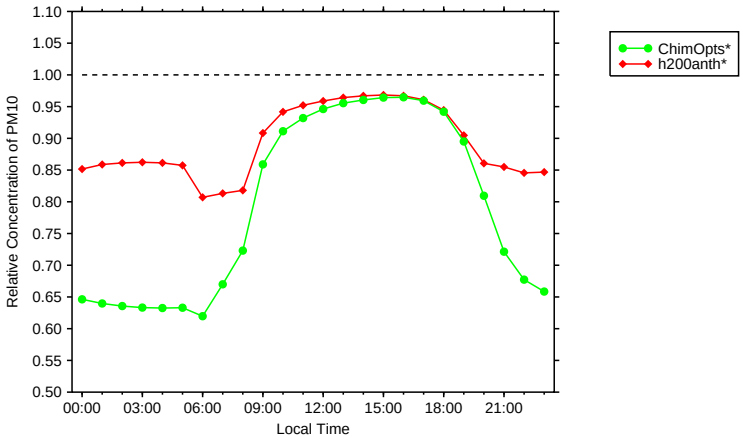

Figure 5.5: Simulation 'ChimOpts' and 'h200anth' are compared to the reference run. They use the nested grid.

Simulation 'ChimOpts' leads to a reduction of about 15% in PM10 concentrations during the night compared to the reference run, see figure 5.5. The measured nocturnal concentrations of PM10 are around 35% lower than the standard run. The difference is due to the out-dated land use data. This data set severely underestimates the urban surface area of Beijing. But this is not the only effect. The nocturnal averaged value for K_z is still lower than $1.0\,m^2$ most of the nights (39 out of 55) and it reaches the minimal value of $0.1\,m^2/s$ almost every night (49 out of 55). Compare this to simulation 'h200anth'. There the nocturnal averaged K_z value is on average around $4.3\,m^2/s$ and only reaches the minimum value of $1.0\,m^2/s$ in 7 nights. This is due to the change in stability. Simulation 'h200anth' has a reduction of nocturnal PM10 concentrations of around 35% which is very close to the observed value. However, this good agreement is partially fortuitous. The anthropogenic heat is still scaled with a too low urban land use percentages and no heat storage is taken into account. Both will increase nocturnal sensible heat flux. However, the heat storage term decreases the daily sensible heat flux, so the reduction seen there will become smaller.

These simulations show that the capability of Chimere to correct for urban areas is very limited. Moreover, the parameters Chimere corrects with, are scaled by the out-dated land use database. Better results are found when more effects are taken into account like the change of stability and when the out-dated land use database is partially corrected for. But still the options to correct Chimere with, without implementing new or better modules, is very limited. Moreover, parameters like anthropogenic heat flux and minimal boundary layer height show an annual cycle, see e.g. [Piringer et al., (2007)] for the annual cycle of boundary layer heights. In winter different values are expected because, for example, the energy used for heating or cooling buildings changes and radiative budgets change. Thus the parameters used in 'h200anth' only work for August and September 2007 and may have to be altered for any other period.

Better results are expected when incorporating in Chimere a boundary layer parameterization which include the most important features of an urban heat island: Anthropogenic heat flux, heat storage and the change in Bowen ratio (the ratio between sensible and latent heat flux). But this is not straightforward and may even be impossible without implementing a meteorological model. This is because the increase in sensible heat flux in reality produces a better mixed boundary layer and thus a different temperature and wind profile. These profiles are the only input for the calculation of the nocturnal boundary layer height meaning it must be adapted in the model as well. However the adaptation of these profiles is not straightforward and their calculation may have to be carried out by a meteorological model.

The best solution in the current setting would be to provide meteo data which already incorporates the heat island effect. In that case, provided that also the land use data is updated, much better results are expected. However, most meteorological models with the resolution and domain used by the standard simulation do not incorporate this effect because it has a marginal effect on meteorological conditions on that scale.

5.4 Conclusions

The urban heat island has a substantial influence on pollutant concentrations in cities. It increases the nocturnal sensible heat flux and thereby it increases the height of the boundary layer, changes its stability and enhances vertical mixing. A case study has shown that a realistic nocturnal boundary layer height in August and September should lie around $150\,m$ to $200\,m$.

Including the urban heat island in Chimere simulations has large effects mostly on nocturnal boundary layers and pollutant concentrations. The nocturnal boundary layer becomes higher and much better mixed so the pollutant concentrations decrease sharply.

Chimere has very limited ways to incorporate this effect when it is not present in the meteo data provided. To correct this implementing a boundary layer parameterization which includes the heat island effect in Chimere should give better results. However, since the effect also has feedback on wind and temperature profiles, it is not straightforward to develop this new boundary layer parameterization. One stringent demand when trying to implement this effect in Chimere is to have an up to date land use database. This database is used to scale the effect with and thus has a substantial influence on the results.

The best way to implement the urban heat island effect in the current setting

is to provide meteorological data which incorporates this effect. However, since the effect on meteorology is small, this data shall probably have to be specially provided.

6 Conclusions & Recommendations

6.1 Conclusions

In this report several sensitivity studies have been carried out to find the reason for the high nocturnal pollutant concentrations in Beijing as modelled by the chemical transport model Chimere when compared to measured values. First it is concluded that PM10 can be used as a tracer to make a change in the dynamics of the model visible. PM10 is chemically not very active and its largest sink, precipitation, does not mask the effect of a change in dynamics.

The sensitivity studies have shown that the model setup as currently used in the operational forecasts of air quality over China within the EU project AMFIC is sensitive to discretization effects. In particular to a shift of the grid and lowering the resolution. The cause is a change in emission distribution when changing resolution or grid definition, without a change in advection or diffusion.

The sensitivity studies have also shown that to effectively decrease nocturnal concentrations of pollutants, the vertical diffusion coefficient (K_z) as well as the boundary layer height should be increased. A physical motivation for this is the influence a city has on its surroundings; the urban heat island effect. The urban heat island effect increases both K_z and the boundary layer height due to increase in sensible heat flux which causes the boundary layer to fail to become stable. Incorporating the effect leads to modelled nocturnal PM10 concentrations which are of the same order of magnitude as the measured ones.

Chimere has limited possibilities to correct for the heat island effect. Including a parameterization for the boundary layer height which incorporates the heat island effect probably leads to better results but may also lead to inconsistencies. The best way is to provide Chimere with meteorological data which already incorporates the heat island effect. However, this may have to be specially provided.

It is stressed that for incorporation of the heat island in Chimere, the land use database needs to be updated. The heat island effect is scaled with the urban land use and thus has a large influence on the result.

It is noted here that daily averaged measurements compare very well with modelled data from Chimere. Measured trends are modelled correctly, however, on average the values are too high by a constant factor.

6.2 Recommendations

It is recommended to use day time surface values from the model as much as possible for as long the urban heat island is not implemented. These are in very good agreement with in situ data from Hong Kong. Daily averages also compare very well to measurements and could therefore also be used provided the correctionfactor is known. Validation with satellite data should, however, always be possible since in this case total columns are used.

Because meteorological data including the heat island effect on the grid used in the current operational forecasts of AMFIC probably has to be specially provided, it is interesting to study if it is possible to let Chimere correct for this. This is however not straightforward, but it may be possible to find an elegant way without introducing very involved calculations. Before any attempt is made

to let Chimere correct for the heat island effect, the land use database should be updated.

For validations it is important to average in situ data over several locations. Because in that case the measurements better represent the concentration of an area. Since the concentration in a surface grid cell should be interpreted as the averaged concentration over the area where it is located, this agrees much better with model data.

Recommendations for further studies: If the precipitation is turned off in the model, the result shows a diurnal cycle when compared to the original data. The effect during the day is more significant than during the night.

When all emissions except in Beijing are turned off, the result shows again a diurnal cycle when compared to the original data. Apparently distant sources have a larger effect on local concentrations during the day compared to the night.

Acknowledgements

I would like to thank Ronald van der A and Bas Mijling, my supervisors at KNMI, for their help and support during my time at KNMI. Their ideas and input for my report have been very helpful. Furthermore I would like to thank Hennie Kelder through whom I've been able to get this assignment for my master thesis. Harry Hoeijmakers, my supervisor from the University of Twente, has given me the opportunity to do this final master assignment externally at the KNMI, I would like to thank him for that.

During my research Gert-Jan Steeneveld, a researcher at the Meteorology and Air Quality Group within the Meteorology and Physical Climatology Section from Wageningen University, has done several simulations for me. Furthermore he was able to answer a lot of questions I had about the subject and he gave me several papers and book references which helped me a lot. I'd like to thank him a lot for that.

Also Karen van de Vel and Wouter Lefebvre from VITO in Belgium have done simulations for me. Unfortunately these haven't made it to the Report because linking these to Chimere proved harder than I thought. But I would like to thank them for their efforts.

I am very grateful that I had the opportunity to attend to the 2009 DRAGON-2 symposium in Barcelona and to present my results. This was financially supported by the EU project AMFIC.

References

[1] [Beljaars, (1995)] Beljaars, A. C. M. (1995) *The Impact of Some Aspects of the Boundary Layer Scheme in the ECMWF model*, ECMWF Seminar Proceedings on Parameterization of Subgrid Schale Physical Processes, reading, U.K., September 1994, 125-161.

[2] [Chen et al., (2009)] Chen, F., M.A. LeMone, M. Tewari, Q. Li, Y. Wang (2009) *An Obsvational and Modeling Study of Characteristics of Urban Heat Island and Boundary Layer Structures in Beijing* Journ. of Appl. Meteo. and Climat. 48:484-501.

[3] [Chimere documentation] Documentation and description of the Chimere model. Freely available at `http://www.lmd.polytechnique.fr/chimere/`.

[4] [Colella and Woodward, 1984] Colella, P. and P.R. Woodward (1984). *The piecewise parabolic method (PPM) for gas-dynamical simulations.* Journal of Computational Physics, 11:38-39.

[5] [Crutzen, (2004)] Crutzen, P., (2004) *New directions: the growing urban heat and pollution 'island' effect—impact on chemistry and climate* Atmospheric Environment, 38:3539-3540

[6] [Cuxart et al. (2006)] Cuxart, J., A.A.M. Holtslag, R.J.Beare, E. Bazile, A. Beljaars, A. Cheng, L. Conangla, M. EK, F. Freedman, R. Hamdi, A. Kerstein, H. Kitagawa, G. Lenderink, D. Lewellen, J. Mailhot, T. Mauritsen, V. Perov, G. Schayes, G-J. Steeneveld, G. Svensson, P. Taylor, W. Weng, S. Wunsch and K-M. Xu (2006) *Single-column model intercomparison for a stably stratified atmospheric boundary layer* Bound.-Layer Meteorol., 118: 273-303.

[7] [Ek et al., (2003)] Ek, M. B., K. E. Mitchell, Y. Lin, E. Rogers, P. Grunmann, V. Koren, G. Gayno, Tarpley, J. D. (2003), *Implementation of Noah land surface model advances in the National Centers for Environmental Prediction operational mesoscale Eta model* Journal of Geophysical Research, 108(D22), 8851, doi:10.1029/2002JD003296.

[8] [Garratt (1992)] Garratt, J.R. (1992). *The Atmospheric Boundary Layer* Cambridge University Press, Cambridge, 316pp.

[9] [Grimmond et al., (2009)] Grimmond, S., M. Blackett, M. Best, with Baik J., Bohnenstengel S., Calmet I., Chemel C., Chen F., Dandou A., Fortuniak K., Gouvea M., Hamdi R., Kondo H., Krayenhoff S., Lee S., Loridan T., Martilli A., Masson V., Miao S., Oleson K., Pigeon G., Porson A., Salamanca F., Shashua-Bar L., Steeneveld G.J., Sugar L., Trombou M., Voogt J., Zhang N., 2009: *The international urban energy balance comparison project: initial results from phase 2*, 29 Jun-3 July 2009, 7th International Conference on Urban Climate,Yokohama, Japan.

[10] [Holton (1972)] Holton, James R., (1972). *An Introduction to Dynamic Meteorology*, Third edition (1992), Academic Press Inc., California, 507pp.

[11] [Holtslag et al. (1998)] Holtslag, A.A.M. and P.G. Duynkerke (1998) *Clear and Cloudy Boundary Layers* Proceedings of the colloquium 'Clear and Cloudy Boundary Layers', Amsterdam, 26-29 August 1997, Royal Netherlands Academy of Arts and Sciences, Amsterdam, 372pp.

[12] [Jacob (1999)] Jacob, Daniel J., (1999). *Atmospheric Chemistry*, Princeton University Press, Princeton, 266pp.

[13] [Kundu and Cohen, (2004)] Kundu, Pijush K. and Ira M. Cohen (2004) *Fluid Mechanics*, third edition. Elsevier Academic Press, San Diego, 759pp.

[14] [Kuska and Kumura, (2004)] Kusaka, H. and F. Kimura (2004) *Coupling a single-layer urban canopy model with a simple atmospheric model: Impact on urban heat island simulation for an idealized case*. Journal of the Meteorological Society of Japan, 82:67-80.

[15] [Lemonsu and Masson, (2002)] Lemonsu, A. and V. Masson (2002) *Simulation of a Summer Urban Breese over Paris* Boundary-Layer Meteorology 104:463-490.

[16] [Mestayer and Anquetin, (1995)], Mestayer, P.G., and S. Anquetin, (1995) *Climatology of Cities*. In: Diffusion of Transports of Pollutants in Atmospheric Mesoscale Flows Fields, Eds: A. Gyr, and F-S Rys. 165-189, Kluwer Acad. Pub, Dordrecht, Netherlands.

[17] [Neu et al., (1994)] Neu, U., T. Knzle, H. Wanner, (1994) *On the relation between ozone storage in the residual layer and daily variation in near-surface ozone concentrations—a case study* Boundary-Layer Meteorology, 69:221-247.

[18] [Oke, (1995)] Oke, T.R. 1995 *The heat island of the urban boundary layer: Characteristics, causes and effects*. In: Wind Climate in Cities, J. E. Cermak et al., Eds., NATO ASI Series E, Vol. 227, Kluwer Academic, 81-107

[19] [Pino et al., (2004)] Pino, D., J. Vilà-Guerau de Arellano, A. Comerón, F. Rocadenbosch (2004) *The boundary layer growth in an urban area* Science of the Total Environment, 334-335:207-213.

[20] [Piringer et al., (2007)] Piringer, M., S. Joffre, A. Baklanov, A. Christen, M. Deserti, K. de Ridder, S. Emeis, P. Mestayer, M. Tombrou, D. Middleton, K. Baumann-Stanzer, A. Dandou, A. Karppinen, J. Burzynski (2007) *The surface energy balance and the mixing height in urban areas — activities and recommendations of COST-Action 715* Boundary-Layer Meteorology, 124:3-24.

[21] [Pope, (2000)] Pope, Stephen B. (2000) *Turbulent Flows* Fourth printing (2006), Cambridge University Press, Cambridge, 771pp.

[22] [Rigby and Roumi, (2008)] Rigby, M. and R. Toumi (2008) *London air pollution climatology: Indirect evidence for urban boundary layer height and wind speed enhancement*, Atmospheric Environment, 42:4932-4947.

[23] [Sarrat et al. (2006)] Sarrat, C., A. Lemonsu, V. Masson, D. Guedalia (2006) *Impact of urban heat island on regional atmospheric pollution.* Atmospheric Environment, 40:1743-1758.

[24] [Souch and Grimmond, (2006)] Souch, C. and Grimmond, S. (2006) *Applied climatology: Urban climate.* Prog. Phys. Geogr., 30:270-279

[25] [Spiegel and Veronis, (1959)] Spiegel, E.A. and G. Veronis (1959) *On the Boussinesq approximation for a Compressible Fluid*, American Astronomical Society, Provided by the NASA Astrophysics Data System.

[26] [Steeneveld et al., (2006)] Steeneveld, G.J., B. J. H. van de Wiel, A.A.M. Holtslag *Modeling the Evolution of the Atmospheric Boundary Layer Coupled to the Land Surface for Three Contrasting Nights in CASES-99.* Journal of the Atmospheric Sciences, 63:920-935.

[27] [Streets, (2008)] Streets, David G., Joshua S. Fu, Carey J. Jang, Jiming Hao, Kebin He, Xiaoyan Tang, Yuanhang Zhang, Zifa Wang, Zuopan Li, Qiang Zhang, Litao Wang, Binyu Wang, Carolyne Yu (2008) *Air quality during the 2008 Beijing Olympic Games*, Atmospheric Environmet, 41: 480-492.

[28] [Stull, 1988] Stull, R.B. (1988). *An Introduction to Boundary Layer Meteorology* Kluwer Academic Publishers, Boston, 666pp.

[29] [Tombrou et al. (2007)] Tombrou, M., A. Dandou, C. Helmis, E. Akylas, G. Angelopoulos, H. Flocas, V. Assimakopoulos, N. Soulakellis (2007) *Model evaluation of the atmospheric boundary layer and mixed-layer evolution* Boundary-Layer Meteorol 124:61-79.

[30] [Troen and Mahrt, 1986] Troen, I. and L. Mahrt (1986). *A simple model of the atmospheric boundary layer: Sensitivity to surface evaporation.* Bound.-Layer Meteorol., 37:129-148.

[31] [Wang et al., 2008] Weng-xing Wang, Fa-he Chai, Kai Zhang, Shu-lan Wang, Yi-zhen Chen, Xue-zhong Wang, Ya-qin Yang (2008), *Study on ambient air quality in Beijing for the summer 2008 Olympic Games*, Air Qual. Atmos. Health (2008), 1:31-36